Extraction, Interpretation and Application of Nonlinear Muscle Synergies toward Proportional Myoelectric Control

著者	Dwivedi Sanjay Kumar
その他のタイトル	比例筋電位制御に向けた筋シナジーの抽出、解釈、および応用の研究
学位授与年度	令和元年度
学位授与番号	17104甲生工第372号
URL	http://hdl.handle.net/10228/00007810

KIT-DD16899030

Doctoral Dissertation

Extraction, Interpretation and Application of Nonlinear Muscle Synergies toward Proportional Myoelectric Control

(比例筋電位制御に向けた筋シナジーの抽出、解釈、および応用の研究)

Dwivedi Sanjay Kumar

February 03, 2020

Department of Life Science and Systems Engineering
Graduate School of Life Science and Systems Engineering
Kyushu Institute of Technology

A Doctoral Dissertation
submitted to Graduate School of Life Science and Systems Engineering,
Kyushu Institute of Technology
in partial fulfillment of the requirements for the degree of
Doctor of Philosophy

Dwivedi, Sanjay Kumar

Thesis Committee:

Professor Shibata, Tomohiro	(Supervisor)
Professor Furukawa, Tetsuo	(Co-Supervisor)
Professor Horio, Keiichi	(Co-Supervisor)
Associate Professor Tamei, Tomoya	(Kobe University)

Extraction, Interpretation and Application of Nonlinear Muscle Synergies Toward Proportional Myoelectric Control*

Dwivedi, Sanjay Kumar

Abstract

Transfer of human intentions into myoelectric hand prostheses is generally achieved by learning a mapping, directly from sEMG signals to the Kinematics using linear or nonlinear regression approaches. Due to the highly random and nonlinear nature of sEMG signals such approaches are not able to exploit the functions of the modern prosthesis, completely. Inspired from the muscle synergy hypothesis in the motor control community, some studies in the past have shown that better estimation accuracies can be achieved by learning a mapping to kinematics space from the synergistic features extracted from sEMG. However, mainly linear algorithms such as Principle Component Analysis (PCA), and Non-negative matrix factorization (NNMF) were employed to extract synergistic features, separately, from EMG and kinematics data and have not considered the nonlinearity and the strong correlation that exist between finger kinematics and muscles. To exploit the relationship between EMG and Finger Kinematics for myoelectric control, we propose the use of the Manifold Relevance Determination (MRD) model (multi-view learning) to find the correspondence between muscular and kinematics by learning a shared low-dimensional representation. In the first part of the study, we present the approach of multi-view learning, interpretation of extracted nonlinear muscle synergies from the joint study of sEMG and finger kinematics and their use in estimating the finger kinematics for the upper-limb prosthesis. Applicability of the proposed approach is then demonstrated by comparing the kinematics estimation

*Doctoral Dissertation, Department of Life Science and Systems Engineering, Graduate School of Life Science and Systems Engineering , Kyushu Institute of Technology, KIT-DD16899030, February 03, 2020.

accuracies against linear synergies and direct mapping. In the second part of the study, we propose a new approach to extract nonlinear muscle synergies from sEMG using multiview learning which addresses the two main drawbacks (1. Inconsistent synergistic patterns upon addition of sEMG signals from more muscles, 2. Weak metric for accessing the quality and quantity of muscle synergies) of established algorithms and discuss the potential of the proposed approach for reducing the number of electrodes with negligible degradation in predicted kinematics.

Keywords:

Electromyography (EMG), muscle activation model, multi-fingered hand, finger joint kinematics, regression, Nonlinear muscle and kinematic synergies, dimensionality reduction

Contents

List of Figures

List of Tables

Chapter 1

Introduction

With the number of active controllable joints in robotic hands and powered prostheses substantially increasing every year, the capability to perform complex movements involving simultaneous control of a large degree-of-freedom (DOF) available in the hand is possible [1]. This makes it possible for the robot devices to generate human-like dexterous manipulation and replicate biomechanically realistic hand movement. Among many potential options, muscle interfacing using surface electromyographic (sEMG) signals is still currently the only viable noninvasive biological signal that can be used to control assistive devices for neurorehabilitation [2], such as active prostheses, or accomplish seamless myoelectric control of many applications.

There are many dexterous robotic hands and hand-prostheses but the difficulty in controlling all available degree-of-freedom (DOF) via myoelectric control has motivated many researchers to focus on more limited control mechanisms. Clinically available EMG-based controllers are only able to control a few DOF at a time [1]. Multiple dimensions have to be controlled sequentially, requiring slow mode-switching mechanisms initiated by different muscle co-contraction. As a result, significant research has been done on pattern recognition-based techniques to output multiple classes of movements, with many studies reaching decoding accuracies of above 95% and classifying up to more than six different hand gestures [3, 4]. Although in these approaches, the number of output movements is still limited and does not provide control of multiple correlated DOFs available in the hand. Current proportional myoelectric control strategies fall short in only being able to control a few numbers of DOFs [5, 6], among other existing limitations listed in [2]. Deployment of proportional and simultaneous

control for multiple DOFs remains one of the major challenges in improving the next-generation myoelectric prostheses and interfaces [7].

Mapping of fine finger kinematic information from sEMG inputs has been done by numerous studies. However, dexterous hand manipulation remains to be one of the most complex biological movements to replicate [8]. This is because the human hand not only has a highly articulated system, with possibly more than 20 kinematic DOF, but also has a complex muscular system involved in the motor control. Indeed a large part of the brain is shown to be devoted to controlling the hand's complex musculo-tendon network [8].

In neurophysiology, it has been argued that synergies control the coordination of muscle recruitment for posture control [9]. The muscle synergy hypothesis claims that the motor system directly initiates movement through flexible combinations of control modules recruited by the central nervous system to simplify control. Similarly, the concept of synergies has also been widely used in the field of robotics, where robot control laws are expressed in low-dimensional space to drive forces applied to the higher dimensional robot space. In motion planning, for example, synergies can often reduce complexity, where searching for an adequate kinematic configuration can increase exponentially with the dimensionality of the structure [10]. Thus, synergies can provide a natural modeling paradigm where muscle activation inputs and high-dimensional joint kinematics can be represented in low-dimensional space, where common latent features are shared. Estimating finger kinematics from sEMG input signals usually involves highly correlated patterns and high dimensionality in both the input and output domains. Nevertheless, few studies have given attention in considering such correlations in doing proportional and simultaneous control of the high dimensional finger kinematics from sEMG signals.

The present study aims at the proportional and simultaneous estimation of finger kinematics from surface EMG by learning an association between muscle and kinematic synergies.

1.1. Research Motivation

This study is inspired by studies in the motor control community that claims that synergistic patterns can be observed in the muscle coordination and posture space. Grinyagin et al. [11] presented different types of synergies. First, static postural synergies, that refer to correlated models between single kinematic poses. Second, kinematic synergies, that consider time-dependent correlation during a motor action task [12]. Lastly, muscle synergies that use recruited muscle coordination patterns from electromyographic (sEMG) activity to address low-level representations of motor control [13–15]. While only the third type of synergy has been largely used in the motor control community, the first two types have inspired a lot of work in robotics[10].

The use of a muscle synergy model together with regression-based methods for robust myoelectric control has inspired a lot of work [5, 16–21]. Studies have shown that muscle synergy features are inherently robust to single-channel electrode shift and amplitude cancellation [6,22].

For better understanding of muscle synergies and their functional role, input spaces such as sEMG or EEG should be studied simultaneously with output spaces such as Kinematics or Force, etc. [23] and studies [24] [25] in the past have also focused in this direction by extracting the components using Nonnegative Matrix Factorization (NNMF) from a dataset containing sEMG and task-related variables. However, the use of NNMF to study a dataset obtained from the concatenation of muscle activations and task-related variables, is not well justified due to the following three reasons.

First, NNMF is a linear decomposition algorithm that may not be able to handle the nonlinearity that exists in sEMG and the corresponding task-related variables. Romero et al. [10] have shown that the postural synergies extracted using linear models failed to represent nonlinear motions even in a simple hand reaching and grasping tasks. Martin et al. [26] have shown that how synergies extracted using linear models failed to extract the agonist-antagonist relationships while synergies extracted using nonlinear models like auto-encoders can represent such information, successfully.

Second, non-negative constraint in the NNMF is suitable for extracting positive coefficients from the muscle activations and giving a physiological interpretation to the extracted components and coefficients but not an appropriate choice for studying the task-related variables which may also have negative values [23].

Third, the number of synergy components chosen are based on the reconstruction

accuracy, in terms of the Variance Accounted For (VAF) or the Pearson Correlation Coefficient (ρ), which are only valid to a certain extent due to the noisy fluctuation in the biological data, instead of capturing task-specific variations in the muscle activity [27]. To understand and extract the task-specific variations from the muscle activity, the relationship between these two (sEMG and finger kinematics) related but different observation spaces has to be analyzed.

To address these issues, in the first part of the thesis, we present the use of the Manifold Relevance Determination (MRD) model to extract nonlinear muscle and kinematics synergies by studying muscle activation and finger kinematic together and their use in estimating finger kinematics from muscle activations input while at the second part we extract muscle synergies only from sEMG data and provide a better alternative than a linear algorithm such as NNMF to the motor control community.

1.2. Research Contribution

This study aims to extract and analyze the nonlinear muscle and kinematic synergies and their application in myoelectric control. The main contributions of this study are as follows:1) To propose a new strategy to extract the relationship between the muscle activations and the corresponding finger kinematics, using the Manifold Relevance Determination (MRD). 2) To present a thorough analysis of the nonlinear muscle and kinematic synergies extracted using the MRD model. 3) To present the use of the acquired synergies to reconstruct the finger kinematics of a full 23-joint skeletal hand model, we show that our estimation method can outperform commonly used regression methods and leads to the intuitive control of multi-fingered prosthesis 4) To present extraction of nonlinear muscle synergies only from sEMG which are consistent over addition of sEMG signals from new muscles which not only provide a better alternative to study co-activation among muscles than a linear algorithm such as NNMF but also gives a possibility to reduce the number of electrodes with only negligible degradation in the predicted kinematics.

1.3. Thesis Overview

This thesis is organized and divided into Five chapters. Chapter 2 presents the related literature and works. Chapter 3 presents the first part of our work, where we propose the use of Manifold Relevance Model (MRD) to understand the relation between muscle activation (input-space) and finger kinematics (output-space). In this work, the acquired nonlinear synergies and the association between them are further used for the estimation of finger kinematics. Chapter 4 presents the second part of our work, where we present a new approach to extract muscle synergies from sEMG data, which provide a better alternative to study the co-activations of muscles than a linear algorithms such as NNMF. Chapter 5 draws some conclusions to our work on in the overall context of synergies and their use in myoelectric control and gives our recommendation and perspective for the future direction of this study.

Chapter 2

Related Work

Each time you take a step, 200 muscles work in unison to lift your foot, propel it forward, and set it down. It's just one of the many thousands of tasks performed by the muscular system: this network of over 650 muscles covers the body and is the reason we can blink, smile, run, jump, and stand upright. So how does it work? Our muscular system is made of three different muscle types namely skeletal, cardiac and smooth muscles. All three kinds of muscles are made of small cells called muscle fiber bundled tightly together. These bundles receives the signal from the central nervous system which contract the muscle fibers and generate force or motion. Due to some unavoidable circumstances, When a person lose a limb, he is no longer able to participate in daily life activities, but the control signals could be recovered from the remaining muscles which could be utilized to transfer the human intentions to the robotic arm. The approach of decoding and transferring the human intentions to the robotic arm, from the electromyography (EMG) obtained from the remaining muscles, is getting significantly better with the advancement of machine learning approaches. This chapter discusses such existing approaches and their drawbacks in detail.

2.1. Myoelectric Controlled Prosthesis

The use of sEMG for controlling prosthetic arms has been started since the 1950s, where the first practical myoelectric controlled prostheses were introduced. Since then, there has been significant research both in control algorithms and robotics. However, most of the clinically and commercially available myoelectric controlled prostheses are based on the principles developed during the early time due to the lack of robustness in state of the art approaches. And that is the reason myoelectric controlled prosthesis suffers from an average rejection rate of 25 percent. Among other reasons of rejections, one of the reasons is the lack of functionality, robust and intuitive control. Users are willing to reconsider the prosthetic arms with enhanced functionality, such as simultaneous and proportional control, individual digit movement, thumb and wrist control, robust and natural control.

With the advancement in machine learning approaches, researchers have applied various classification and regression-based techniques to decode the human intentions from sEMG. Among other features, synergies based features have the potential to provide robust myoelectric control, which took attention of many researchers. Studies have extracted synergies from sEMG using different linear algorithms and used them further for kinematics estimation. One of the classic approach to extract synergies from sEMG has been discussed in the next section.

2.2. Synergy Extraction Methods

The human body has more muscles than joints, which indicates that there are infinite possibilities to perform a given task. To simplify the control mechanism, the Central Nervous System (CNS) might be controlling a group of muscles simultaneously rather than controlling them individually to perform any task. Which gives birth to the idea of muscle synergies. Muscle synergies are usually extracted out of electromyography (EMG) data, which is obtained by placing electrodes on the muscles and recording the electrical activity. To extract the synergies, different matrix factorization algorithms such as Principle Component Analysis (PCA), Independent Component Analysis, And Non-Negative Matrix Factorization (NNMF) can be used. Among all these three algorithms, NNMF is a widely used algorithm in literature to extract muscle synergies.

Because of its property, that factorized matrix cannot have negative values. Hence it provides a physiologically meaningful way to interpret synergy vectors as neurons either firing action potentials (positive) or in resting state (zero).

In this formulation, muscle patterns are assumed to be the linear combination of set of time invariant activation balance profiles with time varying activation coefficient as follows:

$$\mathbf{m} = \sum_{i=1}^{N} \mathbf{c}_i \mathbf{w}_i \tag{2.1}$$

where **m** is a vector that represents multiple EMG channels, **w** contains the synergies or basis functions and **c** represents each activation of each component to the measured muscle activation patterns. See Figure 2.1 to visualize this relationship. In order to

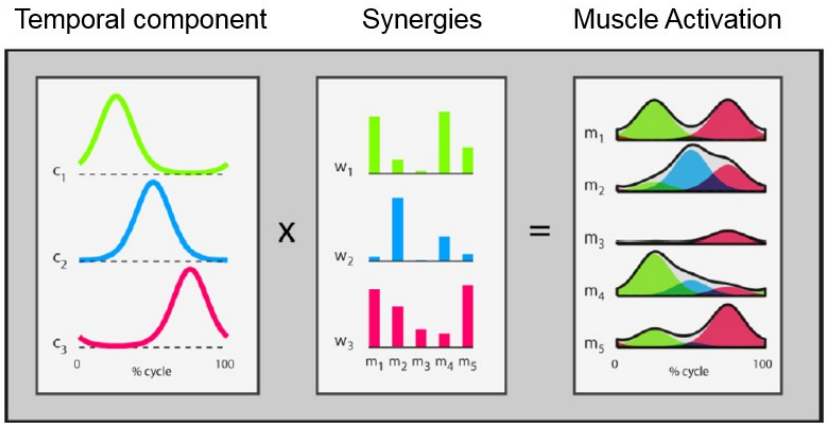

Figure 2.1: Time-invariant synergies capture spatial regularities in the motor output.

find out the optimal number of synergy vectors and also to ensure that the method has learned from the training data sufficiently, the Variance Accounted For (VAF) metric is calculated [28]. The VAF of above 90% across all training points is considered to find good decompositions [29].

2.3. Drawbacks of Synergy Extraction Methods

2.3.1 Unable to Extract Complex Coupling among Muscles

Synergies extracted using NNMF, PCA or any other linear decomposition algorithm are linear in nature and do not capture the inherent nonlinearity that exists in the data.

Spuler et al., have shown it their study by synthesizing the nonlinear nature of data assuming two muscles in an agonist-antagonist relationship as shown in Fig. 2.2. It resembles the activation patterns of biceps and triceps during elbow extension/flexion [26]. This study [26] has demonstrated that the autoencoder (a nonlinear algorithm

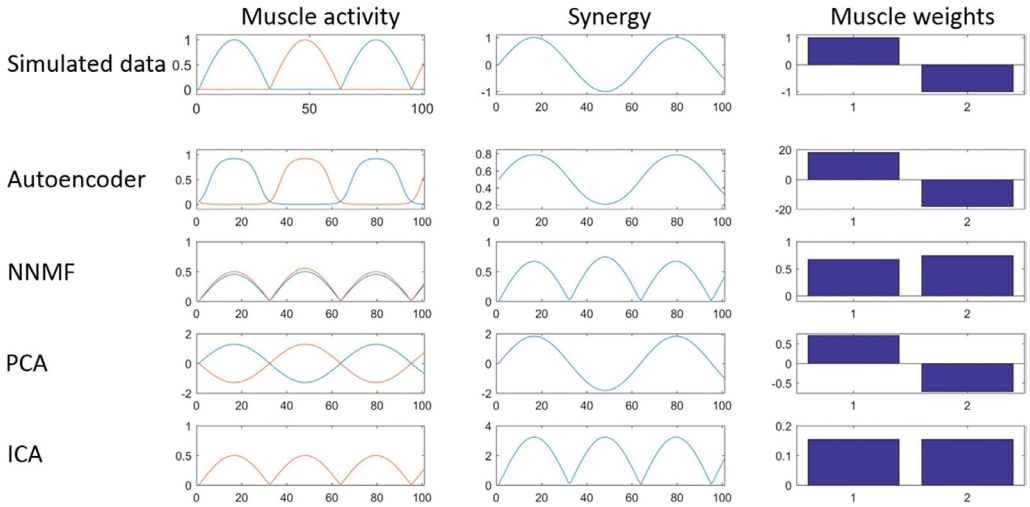

Figure 2.2: Shows the results from [26] in simulated data, which has only one synergy with a sinusoidal pattern. As can be observed from the figure, NNMF and ICA failed to extract the actual synergy pattern, while PCA can only extract synergy but failed to regenerate the actual muscle weights. Only the autoencoder was successfully able to extract both the synergy and muscle weights.

) better models the co-activation of muscles not only in simulated data but also in the real data, collected from the nine subjects when compared with other traditional approaches. This suggests that there is a need to focus on nonlinear algorithms for studying the synergies.

2.3.2 Lack of Functional Meaning

Most of the studies in neuroscience extract synergies from sEMG signals and do not associate them at the task-level. While in robotics, synergies are synthesized at the task-level giving little or no considerations to the biomechanics of human hand. It has

been discussed in great detail, in the study by Alessandro et al. [23], a brief overview is presented over here as follows:

In neuroscience, most of the scientific studies follow these steps to extract muscle synergies:

1. Subjects perform the tasks prescribed by the experimenter.
2. Muscle synergies are extracted from the recorded EMG signals in step 1, applying some linear or nonlinear dimensionality reduction algorithms.
3. Many of the research does not show the reconstruction of tasks from the extracted muscle synergies, which is something missing in the field and need to be addressed.

While in robotics

1. Synergies are synthesized based on the requirements of the desired class of tasks.
2. Then, the synthesized synergies are appropriately combined to generate the motor signals to solve a specific task instance.
3. The quality of the synthesized synergies is finally tested in terms of the obtained task performance.

Studying input space together with the output space will help to associate some functional meaning to the extracted synergies, which in the future could be used for generating human-like motions in a robotic arm provided that the hardware of the robotic hand has similarities with the biomechanics of the human hand. To investigate the relationship between input (sEMG) and output Space (task-level), a joint study of sEMG and finger kinematics has been presented in detail in chapter 3.

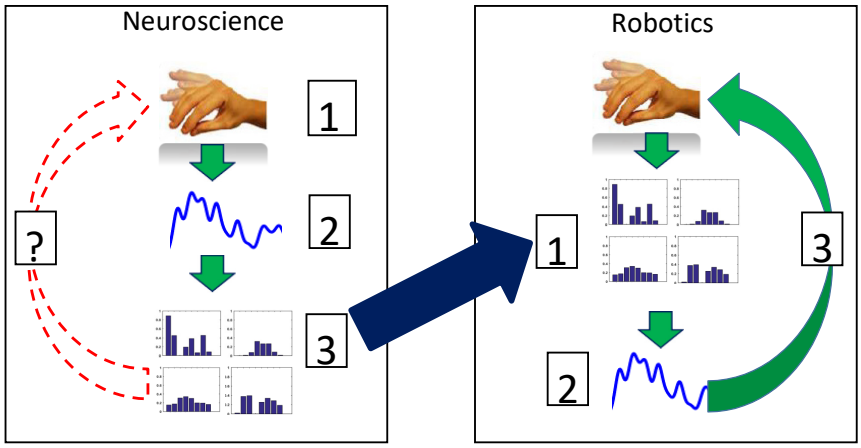

Figure 2.3: Shows the steps $(1-2-3)$ of extracting synergies in neuroscience and robotics. Green arrow shows the flow of steps most of the studies follow in respec-tive fields, while dotted red arrow in neuroscience block indicates the process of re-constructing the task space from the extracted muscle synergies, which is generally avoided in the field of neuroscience, whereas blue arrow indicates the future possi-bility of reusing the muscle synergies in robotics from the neuroscience (a bridge between step 3 in neuroscience to the step 1 in robotics).

2.3.3 Inconsistent Synergistic Structures

In general, EMG is recorded from the surface muscles only, and it is difficult to record the EMG from the muscles beneath the surface muscles. Due to this constraint, Steele et al. [30] have performed a detailed analysis to investigate if the number and choice of muscles impact the result of muscle synergies. They have considered sEMG from a total of 30 muscles. Applying NNMF on the data from all the 30 muscles generated a master set of synergies. While a subset of synergies extracted by ranging the data from 5 to 29 muscles. A similarity metric had been calculated between the subset and master set synergies. This study [30] finds that the structure of synergies is dependent upon the number and choice of muscles included.

To address this problem, a new approach based on multi-view learning has been presented in chapter 4.

Chapter 3

Extraction of nonlinear synergies for proportional and simultaneous estimation of finger kinematics

Proportional and simultaneous estimation of finger kinematics from surface EMG based on the assumption that there exists a correlation between muscle activations and finger kinematics in low dimensional space. We employ Manifold Relevance Determination (MRD), a multi-view learning model with a nonparametric Bayesian approach, to extract the nonlinear muscle and kinematics synergies and the relationship between them by studying muscle activations (input-space) together with the finger kinematics (output-space). This study finds that there exist muscle synergies which are associated with kinematic synergies. The acquired nonlinear synergies and the association between them has further been utilized for the estimation of finger kinematics from muscle activation inputs, and the proposed approach has outperformed other commonly used linear and nonlinear regression approaches with an average correlation coefficient of 0.91 ± 0.03. There exists an association between muscle and kinematic synergies which can be used for the proportional and simultaneous estimation of finger kinematics from the muscle activation inputs. The findings of this study not only presents a viable approach for accurate and intuitive myoelectric control but also provides a new perspective on the muscle synergies in the motor control community.

3.1. Overview

The chapter presents the use of the MRD model to study muscle activation together with the finger kinematics. Firstly, the schematic overview (Fig. 3.1) and formulation of the MRD model to extract the relationship between the muscle activations and the corresponding finger kinematics, using the Manifold Relevance Determination (MRD) [31] is presented. Secondly, the thorough analysis of the nonlinear muscle and kinematic synergies (the shared latent space) extracted using the MRD model from the combined study of muscle activations (input-space) is presented. Finally, we present the use of the acquired nonlinear synergies (the shared latent space) to estimate the finger kinematics of a full 23-joint skeletal hand model. We provide an experimental evaluation that shows how the proposed method outperforms commonly used linear and nonlinear regression approaches, in terms of estimating finger kinematics using muscle activation inputs.

3.2. Methods

In this section, we present the MRD model [31] and its formulation, used for finding the nonlinear muscle and kinematic synergies and the interaction between them (shared latent space). First, the MRD model and its formulation is presented. The inference algorithm is then described, which is used to estimate finger kinematics from sEMG using the obtained shared latent space. Finally, the implementation details of the linear regression and artificial neural network are presented, which are later used in the study to compare the estimation performance of the MRD model.

3.2.1 Manifold Relevance Determination(MRD)

Gaussian processes (GPs) are powerful models that can be used for classification or regression that incorporates numerous classes of function approximators [32]. Lawrence proposed the Gaussian Process latent variable model (GPLVM) as a new technique for nonlinear dimensionality reduction that uses Gaussian processes (GPs) to find a nonlinear manifold to preserve the variance of the data in a latent space representation [33]. Several studies have been proposed to handle multi-view learning. For example, Shon et al. proposed a generalization of the GPLVM that represents multiple observation

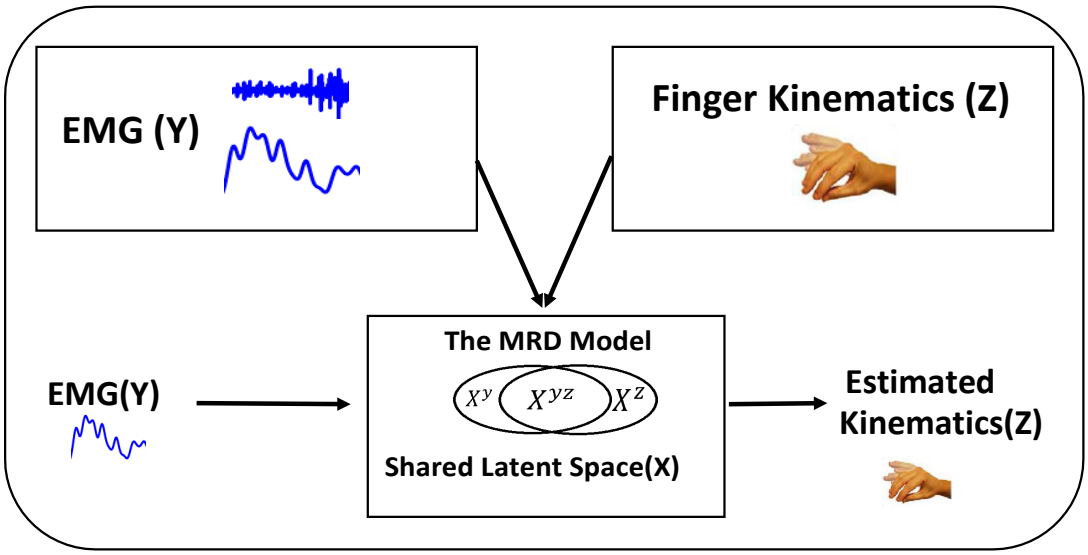

Figure 3.1: Schematic overview of the proposed method for extracting the nonlinear muscle and kinematic synergies and their relationship, using the MRD model. Two different but related observation spaces, namely sEMG (Y), recorded from eight muscles in the forearm and the corresponding 3D coordinates of 23 joint marker positions in the hand (Z), which include three set of tasks, namely: (1) individual finger flexion-extension (IFFE), (2) all finger flexion-extension (AFFE), and (3) random flexion-extension of one or more fingers (RFFE), are given to the MRD model as input. The learned shared latent space (X) is comprised of three subspaces. First subspace (X^y) represents the independent muscle synergies, second subspace (X^{yz}) represents the association of muscle and kinematic synergies while the third subspace (X^z) which would represent the independent kinematic synergies, is rarely observed, in this study.

spaces that are linked via a single shared latent variable model [34]. Ek et al. presented a factorized latent variable model where the shared and individual variances of two correlated observation data were represented in separate subspaces [35]. In these previous methods, however, the dimensionality of the latent spaces was heuristically set, and inference for new test data points had to rely on maximum a posteriori (MAP) search in the latent space. To overcome these limitations, Damianou et al. [31] proposed a full Bayesian factorized latent variable model based on GPLVM that allows for the automatic estimation of dimensionality of the latent space, and provides an approximation to the full posterior of the latent points given the data. In this study, we

follow the same approach.

The problem is formulated as follows: Given that we have two observation data $Y \in \mathsf{R}^{N \times D_Y}$ and $Z \in \mathsf{R}^{N \times D_Z}$, the goal of the model is to find a factorized latent variable parameterization in a space $X \in \mathsf{R}^{N \times Q}$ that relates corresponding pairs of observations from different spaces Y and Z. It is assumed that the two datasets are generated from a low dimensional manifold mapped from smooth functions $\{f_d^Y\}_{d=1}^{D_Y} : X \to Y$ and $\{f_d^Z\}_{d=1}^{D_Z} : X \to Z$ ($Q << D$), corrupted by noise:

$$\begin{aligned} y_{id} &= f_d^Y(\mathbf{x}_i) + \varepsilon_{id}^Y \\ z_{id} &= f_d^Z(\mathbf{x}_i) + \varepsilon_{id}^Z, \end{aligned} \tag{3.2}$$

where $\{y, z\}_{id}$ represents dimension d of sample point i and ε_{id}^Y, ε_{id}^Z are sampled from a zero mean Gaussian distribution. This leads to the likelihood under the model, $P(Y, Z | X, \vartheta)$, where where $\vartheta = \{\vartheta^Y, \vartheta^Z\}$ contains the parameters of the mapping functions and noise variances. Finding the latent representation X and mapping functions f^Y and f^Z is an ill-constrained problem. Lawrence provided a solution by placing GP priors over the mapping and the resulting model is the Gaussian Process Latent Variable Model (GPLVM) framework [33]. In this framework, each generative mapping is modeled as a product of independent GP's parametrized by the kernel or covariance function $K = \{K^Y, K^Z\}$ evaluated over the latent variable X, so that

$$P(F^Y | X, \vartheta^Y) = \prod_{d=1}^{D_Y} N(\mathrm{f}_d^Y | \mathbf{0}, K^Y), \tag{3.3}$$

where $F^Y = \{\mathrm{f}_d^Y\}_{d=1}^{D_Y}$ with $f_{id}^Y = f_d^Y(\mathbf{x}_i)$, and similarly for F^Z. This allows the general nonlinear mapping function F to be marginalized out leading to a likelihood function in the form of a product of Gaussian densities:

$$P(Y, Z | X, \vartheta) = \prod_{K=\{Y,Z\}} \int p(K | F^K) p(F^K | X, \vartheta^K) dF^K \tag{3.4}$$

Integration over (4) is then done by variationally marginalizing out X by using variational approximation techniques used for standard GPLVMs. A non-standard but analytical solution through variational learning techniques and using induced variables is described in [31, 36, 37]. The shared latent space (X) is composed of three subspaces, representing the shared and private variance for each observation data, $X = \{X^Y, X^{YZ}, X^Z\}$. Bayesian training automatically allocates the dimension of this

shared latent space (X) using automatic relevance determination (ARD) priors [31]. In the automatic allocation of the dimensionality, the dimensions D_Y and D_Z of the latent functions f^Y and f^Z, respectively, are selected to be independent draws of a zero-mean GP with an ARD kernel or covariance function with the following form:

$$k^{\{Y,Z\}}(\mathbf{x}_i, \mathbf{x}_j)_{ard} = (\sigma^{\{Y,Z\}})^2 e^{-\frac{1}{2}\sum_{q=1}^{Q} w_q^{\{Y,Z\}}(x_{i,q}-x_{j,q})^2}. \tag{3.5}$$

where $w_q^{\{Y,Z\}} = \alpha(l_q^{\{Y,Z\}})^{-2}$, with α a constant positive scale value and length scales l. Although a common distribution for X is learned, two sets of ARD weights $W = \{\mathbf{w}^Y, \mathbf{w}^Z\}$ are obtained to automatically infer the relevance of each latent dimension for generating points in the Y and Z spaces respectively. The latent shared subspace $X^{YZ} \in \mathbb{R}^{N\times Q_S}$ is then defined by the set of dimensions $q \in [1, \cdots, Q]$ for which $w_q^Y, w_q^Z > \delta$, with δ close to zero and $Q_S \leq Q$. As for the two private spaces, X^Y and X^Z, these are also inferred automatically along with their corresponding dimensionalities, Q_Y and Q_Z, respectively. More specifically:

$$X^Y = \{\mathbf{x}_q\}_{q=1}^{Q_Y} : \mathbf{x}_q \in X, w_q^Y > \delta, w_q^Z < \delta. \tag{3.6}$$

and analogously for X^Z. This model is summarized in the graphical model shown in Fig. 3.2. The Bayesian GPLVM Matlab toolbox [38] was used to implement the model training and dimensionality relevance determination in this study.

Inference Algorithm

To predict finger kinematics from sEMG, the nearest neighbor approach (NN) to search for a similar point in the training data for the given sEMG was used, details of which explained in algorithm 1.

Algorithm 1 Inference of Finger Kinematics *Z*, given sEMG *Y*

1: *Given* : MRD model trained on two views (Y, Z)
2: *Given* : A test point y_*
3: Find $y_{train} = NN(Y_{train}, y_*)$
4: Select $x_*(x_*^y, x_*^{yz}, x_*^z)$ from $X\,(X^y, X^{yz}, X^z)$ corresponding to the index of y_{train}
5: Find $x_*^{ss} = NN(X_*^{yz}, x_*^{yz})$
6: Predict $z_* = P(Z|x_*^{ss})$

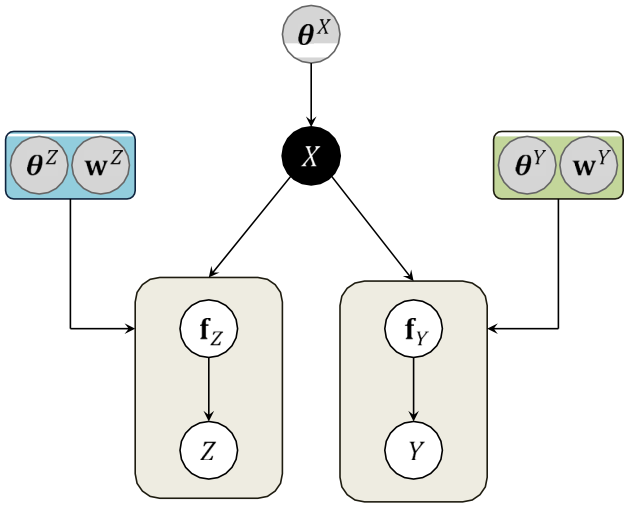

Figure 3.2: Graphical model of the MRD model. A distribution for shared latent space X is learned and the hyperparameters $\mathbf{w}^{Y,Z}$ and $\vartheta^{Y,Z}$ are the ARD weights that determine the dimensionality and the function model parameters, respectively.

3.2.2 Linear Regression (LR)

A simple linear regression has been performed between muscle activations and finger kinematics using the MATLAB "¥" operator. Simple linear regression in the MATLAB considers only one independent variable (x) as :

$$y = mx + c + \varepsilon \tag{3.7}$$

where y is the response variable, c is the y-intercept, m is the slope (or regression coefficient), and ε is the error term.

3.2.3 Artificial Neural Network (ANN)

ANN has been implemented using the fitnet function of MATLAB with default training algorithm Levenberg-Marquardt ('trainlm') from the Netlab toolbox. The network is made of an input layer, a hidden layer with a tan-sigmoidal activation function, and a single linear output layer. The number of neurons in the hidden layer is set to be the 2/3 of the sum of the neurons in the input and output layer. Parameters of the network were obtained by minimizing a mean square error function. A single network is used

to simultaneously and continuously estimate the finger kinematics from the muscle activations.

3.3. Datasets

3.3.1 Data Collection

Surface EMG signals were extracted from eight extrinsic muscles of the hand that known to contribute to the wrist and finger movements (Fig. 3.3). Bipolar active-type Ag-AgCl electrodes, with an inter-electrode distance of 20 mm, were placed on the extrinsic muscles of the forearm. The target muscles and the related finger movements are listed in Table 3.1. These target muscles were mostly found by palpation and commonly known anatomical landmarks described in [39]. A single electrode was also placed on the subject's olecranon to serve as ground and reference electrode.

The sEMG signals were measured using a compact BA1104 pre-amplifier and a TU-4 telemetry unit (Digitex Lab. Co. Ltd). The hardware provided a high-frequency filter of 1 kHz during the sEMG data acquisition process. The sEMG signals were sampled at 2 kHz, and were digitized by an A/D converter with 12-bit precision. The

Table 3.1: Selected sEMG channels and the target muscles

C	Target Muscle	Hand/Finger
1	Abductor pollicis longus(APL)	Thumb abduction,extension
2	Flexor carpi radialis(FCR)	Wrist, hand flexion
3	Flexor digitorum superficialis(FDS)	2-5th finger PIP flexion
4	Flexor digitorum profundus(FDP)	2-5th finger DIP flexion
5	Extensor digitorium(ED)	2-5th finger extension
6	Extensor indices(EI)	Index finger
7	Extensor carpi ulnaris(ECU)	Wrist extension and abduction
8	Extensor carpi radialis(ECR)	Wrist and thumb

Source: Anatomy and Kinesiology of the Hand [40].

sEMG signals were displayed on a real-time monitor and visually inspected to check its quality. Along with the sEMG signals, unconstrained and continuous wrist and finger movements were also simultaneously recorded using a MAC3D motion capture system (Motion Analysis Corp.). Twenty-three passive reflective markers were attached on the subject's hand (see Fig. 3.3), one on each joint and tip of the finger, three in the wrist area and one in the forearm for reference. The Cortex software from Motion Analysis was used to concurrently record and synchronize the sEMG and motion data. The marker positions were recorded at 200 Hz sampling rate with measurement units in millimeters (mm). The full hand kinematic dimension is given by the 23-marker hand skeleton model 3D information in the motion capture space. Later on, the metacarpophalangeal (MCP), the proximal interphalangeal (PIP) and the distal interphalangeal (DIP) joint angles were also calculated from the recorded marker positions following the procedure described in [41]. Because the thumb does not have a DIP joint, the carpometacarpal (CMC) joint was considered. These joint angle values are used in EMG-to-Muscle activation model.

The total data used included those of 10 healthy and intact participants (9 Male, 1 Female, aged 26-31 years old). The subject, seated with their dominant hand and elbow comfortably positioned on a flat surface table, were asked to do different flexion and extension finger movement tasks which includes the following:

1. Individual finger flexion-extension (IFFE)
2. All finger flexion-extension (AFFE)
3. Random flexion-extension of one or more fingers (RFFE)

In the first task, the subject was asked to move one finger at a time, in the flexion-extension plane of each finger. The second task involved the subject moving all fingers simultaneously, in the same flexion-extension plane. This motion resembled the opening and semi-closing of the hand. Full closing of the hand was not possible as some markers at the tip of the fingers would not be seen by the motion capture system. In these first two tasks, the subjects mainly did MCP flexion and extension, in which the PIP and DIP followed the movements of the MCP joint. Finally, for the third and last part of the experiment, the subject was asked to move any finger freely in any direction within the motion capture volume space while still maintaining a fixed neutral position for the arm and elbow. Irregular movements and different finger combinations for

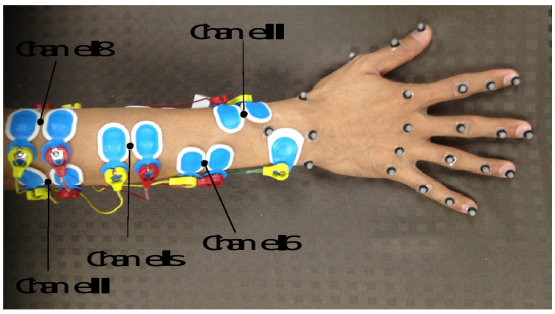

Figure 3.3: General overview of electrode placement in the forearm

flexion and extension movement were encouraged from the subject in this last part of the experiment. However, in this task fingers barely reached to maximum flexion or extension.

The first task consisted of 5 sets of movement, one for each finger. While the remaining tasks consisted of 1 set each. Each set consisted of 5 trials with each trial lasting 20 seconds. All the movements were limited to finger flexion and extension movements while the rest of the arm (e.g. wrist, elbow, etc.) maintained a fixed position upon instruction. Markers on the wrist joint were also recorded to ensure that the wrist maintained a fixed position, or at least minimal ulnar/radial angle deviation. A ringing sound, from the motion capture device, signaled the start and end of a trial in the experiment. All the trials were sequentially done and the participants were allowed to rest anytime throughout the experiment. The subjects could make as many movements but were instructed to move in their own perceived normal velocity ($\leq$ 2 cycles of movement per second) and to maintain the least amount of wrist ulnar/radial angle deviation. The subjects were tasked to reach maximum flexion and extension for each finger at least once at any point in any of the trials. There was no obstacle or object to impede/induce force in the experiment. A video demonstration (Recorded_Kine.mp4) of the recorded finger kinematics corresponding to all three tasks are provided in the supplementary material. This dataset is available online at IEEE DataPort as open access datasets [42].

3.3.2 Data Preprocessing

EMG-to-Muscle activation model

The raw sEMG signals were first preprocessed into a form, that after further manipulation, can be used to estimate muscle activation [43,44]. An EMG-to-Muscle Activation model is used to consider the effects of electromechanical delay (EMD) and activation dynamics in place of sEMG delay lines. It has been shown in previous studies, that using this feature works very well in estimating muscle force [45] and finger kinematics [46].

The raw sEMG signals were digitally band-pass filtered in the range of [10, 500] Hz using a 4th-order Butterworth filter. The sEMG signals were then rectified, normalized by the overall peak rectified sEMG obtained, low-pass filtered (4 Hz cut-off frequency, zero-phase, 4th-order Butterworth filter) and downsampled to match the frequency of the motion data.

Buchanan et al. proposed a second-order model filter that works more efficiently to model the relationship between sEMG and muscle activation [43, 44]. In this study, we employed such a filter to obtain muscle activation $u_j(t)$ given by:

$$u_j(t) = \alpha e_j(t-d) - \beta_1 u_j(t-1) - \beta_2 u_j(t-2) \tag{3.8}$$

$$v_j = \frac{e^{A_j u_j(t)} - 1}{e^{A_j} - 1} \tag{3.9}$$

where $e_j(t)$ is the rectified, normalized and filtered sEMG of muscle j at time t. In this model, α, β_1, β_2 are recursive coefficients of the filter, d is the EMD parameter and A handles the nonlinearity parameter of the activation feature. Filter stability is guaranteed by subjecting α, β_1, and β_2 to the following constraints:

$$\beta_1 = \gamma_1 + \gamma_2 \tag{3.10}$$

$$\beta_2 = \gamma_1 \cdot \gamma_2 \tag{3.11}$$

$$|\gamma_1| < 1, |\gamma_2| < 1 \tag{3.12}$$

$$\alpha - \beta_1 - \beta_2 = 1 \tag{3.13}$$

The muscle activation model parameters are obtained using a linear regressor and optimized through constrained nonlinear programming using the Matlab Optimization

Toolbox by minimizing the following cost function:

$$\frac{1}{N_t}\sum(Z_{\text{ANGLE EST}} - Z_{\text{ANGLE TARGET}})^2 \tag{3.14}$$

where N is the total number of training samples, and $Z_{\text{ANGLE EST}}$ and $Z_{\text{ANGLE TARGET}}$ are the estimated and calculated finger joint angles, respectively.

Finger Kinematics

The motion data, on the other hand, were also low-pass filtered (4 Hz cut-off frequency) to remove any jitters. In this study, a factorized latent representation X is extracted from the 8-channel muscle activation input $Y \in \mathbb{R}^{N\times 8}$ and from the 23-marker finger posture $Z \in \mathbb{R}^{N\times 69}$. We considered all the 3D information on each marker which summed up to a total of 69 dimensions in the hand kinematic space.

3.3.3 Training Data to the Models

All the models are separately trained for each subject and for a subject there are in total 140，000 sample data points ($\mathbb{R}^{140,000\times 8}$ and $\mathbb{R}^{140,000\times 69}$ for muscle activations and finger kinematics, respectively) from three sets of tasks corresponding to all five trials.

MRD Model

For Synergistic Analysis Data points from all five trials of task 1 (IFFE) and task 2 (AFFE) combined together, shuffled and then further downsampled by a factor of 30. Downsampling is done because training the MRD model is computationally expensive for large datasets, but handles data with large dimensions very well. 70% of the downsampled dataset is used as training data, while the full dataset (around 136,000 data points) without down-sampling except the training data are used as test data.

For Synergistic Analysis, task 3 (RFFE) have not been included in the model training as the motions were random across the trials and subjects, and may pose difficulties in the interpretation and comparison of the obtained synergy components across the subjects.

For Finger Kinematics Estimation To check and compare the estimation capability of the nonlinear synergistic features obtained from the MRD model with other commonly used approaches, new sets of MRD models were trained for each subject, but now including the data from all three tasks, keeping rest of the training and test procedure same as used for synergistic analysis. The effect of including the third task in the training data over extracted synergistic patterns has been analyzed and presented in discussion section.

Artificial Neural Network (ANN) and Linear Regression (LR)

Data points from all the five trials and three set of tasks were combined together, shuffled and then further down-sampled by a factor of 30. Similar to the MRD model, 70% of the down-sampled dataset is used as training data, while the full dataset (around 136,000 data points) excluding the training points are used as the test data.

As the MRD model makes use of reduced dimensions (shared latent space) to map data from one view into another, both of these models (ANN and LR) were also trained on reduced dimensions obtained after applying Principle Component Analysis (PCA) on each of the downsampled datasets.

The number of reduced dimensions or principal components was selected based on 90% total accumulated data variance. Five and nine principal components were needed to explain 90% of the data variance in the sEMG and finger kinematics data, respectively. Predicted data points were recovered back to the original space to evaluate the performance metrics.

For ANN and LR, the down-sampling of the dataset has been done to keep the number of training data points similar to that of the MRD model. Increasing the training samples [46], using the deep neural network architecture Or creating a dedicated MLP for each DOF [47] may lead to better estimation performance, but how large the training data is required or how deep the network architecture should be or to what extent retraining the model is needed, has not been investigated in this study.

As the focus of the study is to provide a data efficient approach to extract and interpret the nonlinear synergy components by studying sEMG (input space) together with the task-related variables (output space) and their application in estimating finger kinematics.

3.3.4 Performance Evaluation Metrics

The quality of estimated finger kinematics is evaluated using the three metrics namely root-mean-square error (RMSE), Correlation Coefficient (ρ) and R-square.

$$\mathrm{RMSE}_i = \sqrt{\frac{\sum_{t=1}^{N} (Z_{\mathrm{MEASURED}} - Z_{\mathrm{EST}})^2}{N}} \tag{3.15}$$

where Z_{MEASURED} and Z_{EST} are the measured and estimated x, y and z coordinates of the 23 marker positions, respectively. The value of N would be 69. The RMSE performance index gives the square root of the mean of the square of all of the error. Compared to other error metrics, RMSE amplifies and severely punishes large errors. The other two performance metrics, correlation Coefficient (ρ) and R-square are also calculated between Z_{MEASURED} and Z_{EST}.

3.4. Results

This section first describe the latent space obtained after applying MRD on EMG (input-space) and kinematics (output-space) separately. Then the the shared latent space (X) and its synergistic interpretation is discussed when analyzing EMG (input-space) together with the kinematics (output-space) using the MRD model and then the proportional and simultaneous estimation of finger kinematics from surface EMG signals using shared latent space (X) is presented. The dataset obtained from subject 1 (S1) is used for visualization of results. Significant improvement in the estimation of the finger kinematics is achieved, when compared with other regression methods as shown later in Table 3.3.

3.4.1 Analyzing EMG and Kinematics Separately

To find a latent space based only on the EMG dataset, 8 dimensional EMG data are given as input to the Bayesian GPLVM model (MRD on one view). Initially the dimensionality of the latent space is set equal to the dimensionality of the original EMG space because Automatic Relevance Determination (ARD) procedure in BGPLVM sets the weight (inverse length scale) of a latent dimensions almost close to zero when it has no significance in reconstructing the higher dimensional space, while higher weights

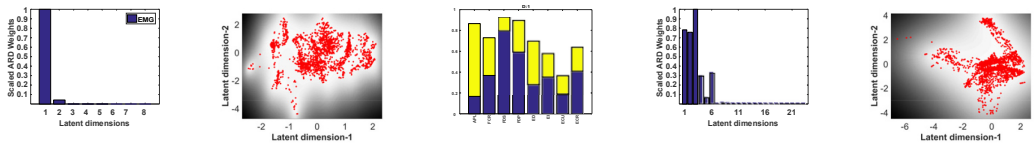

(a) (b) (c) (d) (e)

Figure 3.4: Shows the latent spaces for EMG and kinematics obtained using the Bayesian GPLVM (a) shows the scaled ARD weights for each dimension in the latent space corresponding to the EMG while (b) shows the projection of latent space into dimension $\{1$ and $2\}$. (c) Shows the muscle activations values obtained by following the procedure of sampling latent points along the dimensions 1 as shown in dotted blue line in (b). Yellow bar on the top of blue bars indicates the amount of modulation in the activation values with respect to the first point when moving from left to right in (b).

are assigned for relevant dimensions. Fig. 3.4a shows the scaled ARD weights with respect to each latent dimension. It is clear from Fig. 3.4a that latent dimension $\{1$, and $2\}$ are of significant importance while other latent dimensions can be omitted for further analysis. Fig. 3.4b shows the projection of the latent space into dimension $\{1$, and $2\}$. The red dots in Fig. 3.4b correspond to the posterior mean of each training data points projected onto a 2D space, while the gradient of the background corresponds to the posterior variance (white for low variance and black for high variance). Encoded information in a latent dimension can be understood by sampling new latent points along that dimension, and mapping the sampled latent point (X_{samp}) to the higher dimensional space by calculating the likelihood $P(Y|X_{samp})$.

Latent dimension $\{1\}$ in 3.4a has been investigated by mapping the muscle activations corresponding to the sample latent points along the dimension 1 as shown by dotted blue line in 3.4b while keeping the points fixed corresponding to the other latent dimensions. Fig. 3.4c shows the obtained muscle activations corresponding to the sample latent points. Blue bars on the top of the yellow bars shows the modulation in the activation values when moving from left to right in Fig. 3.4b along the blue line, while yellow bars shows the activation values at the left most point.

Similarly, Fig. 3.4d shows the ARD weights corresponding to 23 latent dimensions obtained after applying BGPLVM separately on 69 dimensional kinematics data. Six

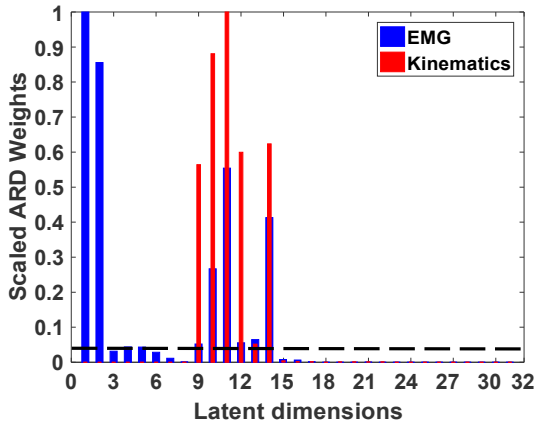

Figure 3.5: The shared latent space (X) obtained using the MRD model, it shows the scaled ARD weights corresponding to every latent dimension in X. Dimensions $\{1, 2\}$ represents the subspace, private to sEMG (X^y), while dimensions $\{9, 10, 11, 12, 13$ and $14\}$ represents the shared subspace (X^{yz}) between sEMG and the finger kinematics,

significant latent dimension $\{1,2,3,4,5$ and $6\}$ are considered for further analysis. A similar process of reconstructing the higher dimensional space from sampled latent point along a dimension has been used to find the encoded kinematics motion in those six significant latent dimension. Recovered finger motions for latent dimensions are as follows: 1. AFFE, 2.Middle, Ring+Little, 3. Ring, Index 4. AFFE and Thumb.

3.4.2 Shared Latent Space Obtained using the MRD Model

To find the shared latent space (X) between the sEMG and the finger Kinematics, eight muscles activations and the corresponding 3D coordinates of the 23 joint marker positions, are given as inputs to the MRD model. To ensure that the model finds the correspondence between the two spaces if and only if it exists, the dimensionality of the latent space (X) is set to the sum of the dimensionality of the original spaces, i.e. $8 + 23 = 31$, in spite of the fact that the dimensionality of the latent space (X) could be much lower because of the inherent correlation that exists in the dataset. The model automatically finds the relevance of every dimension in latent space (X) using the ARD procedure by assigning higher ARD weights to relevant dimensions, and making

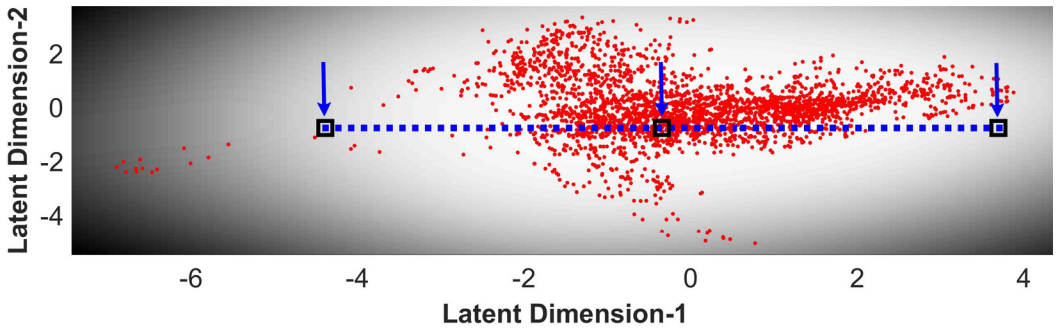

(a)

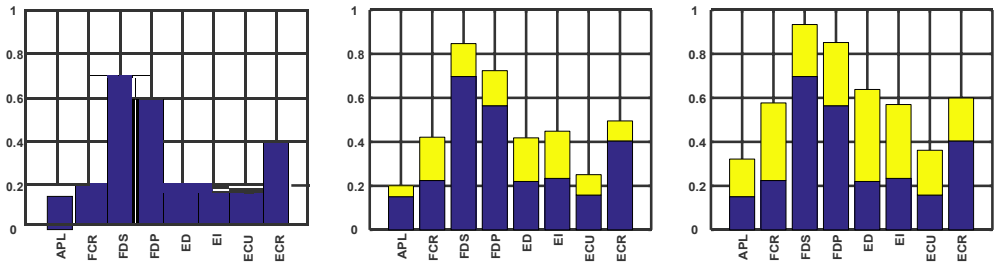

(b)

Figure 3.6: Sample investigation process to find encoded information in the latent dimensions, (a) shows the projection of latent space into dimensions $\{1$ and $2\}$, and a sample process to find the encoded information in a latent dimension. Muscle activation values corresponding to dimension $\{1\}$ can be obtained by sampling the latent points along it as shown by the dotted blue line, while keeping the points fixed on the other dimensions. Visualization of muscle activation values corresponding to the three latent points, indicated by the blue arrow, are shown in (b). Yellow bars on the top of blue bars indicate the amount of modulation in the activation values with respect to the first point when moving from left to right in (b).

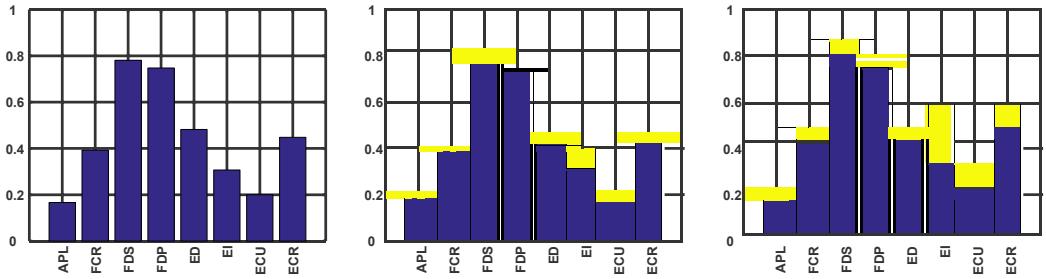

(a)

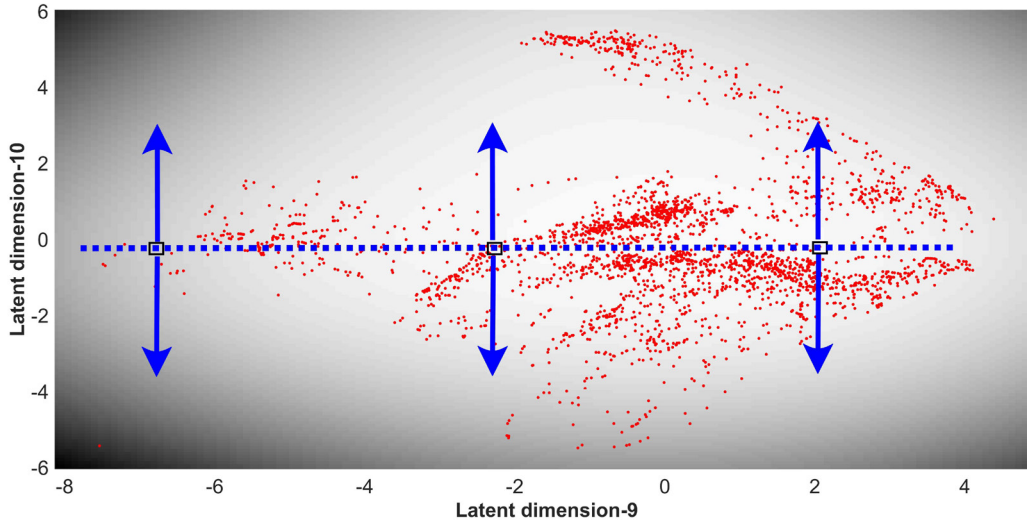

(b)

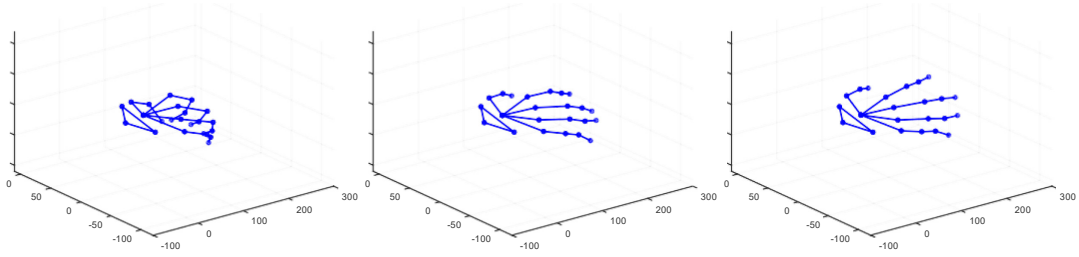

(c)

Figure 3.7: Exploration of couped latent dimension in the shared latent space (X), (b) shows the projection of latent space (X) into dimensions $\{9, 10\}$. When sampling the latent points along the dimension $\{9\}$ as shown by the dotted blue line, proportional and simultaneous estimation of flexion and extension of all fingers along with related muscle activations is achieved. The visualization of muscle activations and finger kinematics corresponding to the six latent points, indicated by the blue arrow, are shown in (a) and (c), respectively.

it close to zero when there is little relevance, as such high dimensionality of the latent space, in the beginning, will not be a problem either.

Fig. 3.5 shows the scaled ARD weights for all 31 dimensions of the latent space (X) obtained using the MRD model. The threshold is set to 0.04 as shown by the dotted black line, leads to six significant dimensions $\{1,2,9,10,11,12,13 \text{ and } 14\}$ which are considered for further investigations. Dimensions $\{1 \text{ and } 2\}$ represents the subspace (X^{y}), which is private to sEMG space and dimensions $\{9,10,11,12,13 \text{ and } 14\}$ represents the shared subspace (X^{yz}) between sEMG and the finger kinematics, while dimensions representing the subspace private to finger kinematics (X^{z}), can rarely be seen, which is a consistent trend across all subjects.

A dimension in latent space (X) represents either only a muscle synergy, or only a kinematic synergy, or a coupling of both synergies. Encoded information in a latent dimension related to sEMG or finger kinematics can be understood by sampling new latent points (X_{samp}) along a dimension, and mapping them to the related higher dimensional spaces by calculating the likelihood $P(Y|X_{samp})$ or $P(Z|X_{samp})$.

Muscle Synergies Independent of Kinematic Synergies

Latent dimensions $\{1 \text{ and } 2\}$ represent the muscle synergies that are independent of finger kinematics. Fig. 3.6a shows the projection of the latent space into dimension $\{1, \text{ and } 2\}$. The red dots in Fig. 3.6a corresponds to the posterior mean of each training data points projected onto a 2D space, while the gradient of the background corresponds to the posterior variance (white for low variance and black for high variance).

Encoded muscle activation values in the dimension $\{1\}$ are obtained by sampling the latent points along with it (the dotted blue line), while keeping the values fixed corresponding to other latent dimensions. Visualization of muscle activation values corresponding to three latent points, indicated by the blue arrow in Fig. 3.6a, are shown in Fig. 3.6b. Yellow bars on the top of blue bars indicate the amount of modulation in the activation values with respect to the first point when moving from left to right in Fig. 3.6a. Similarly, the activation values corresponding to the latent dimension $\{2\}$ can also achieved.

However, the presence of second latent dimension private to sEMG space was not consistent across the subject and have not been considered for further analysis.

Table 3.2: Encoded kinematics in latent dimensions for 10 subjects

	9	10	11	12	13	14	15
S1	AFFE	Middle	Ring	Index	Thumb	Thumb	—-
With RFFE	AFFE	Middle	Ring	Index, Little	Thumb	Thumb	—-
S2	AFFE	Ring+Little	Thumb	Middle+Ring+Thumb	Index	—-	—-
With RFFE	AFFE	Ring+Little,Thumb	Thumb+Middle	Index, Middle+ring		—-	—-
S3	AFFE	Ring+Little	Middle	Thumb+Index	Middle+Ring	—-	Thumb
With RFFE	AFFE	Ring+Little	Middle	Ring	Thumb+Index+Ring	—-	—-
S4	AFFE	Middle+Ring	Ring+Little+Thumb	Thumb	Thumb+Index	—-	–
With RFFE	AFFE	Middle+Ring	Ring+Little+Thumb	Thumb	Thumb+Index	—-	–
S5	AFFE	—-	Middle	Ring	Thumb,Index	—-	Thumb
With RFFE	AFFE	—-	Middle+Ring	Ring+Little	Similar to AFFE	Thumb+Little	—-
S6	AFFE	Thumb	Middle+Ring+Little+Thumb	Little	—-	Ring	—-
With RFFE	AFFE	Thumb	Thumb	Ring+Little	Middle+Ring	Ring	AFFE
S7	AFFE	Ring+Little	Middle	Index	—-	—-	—-
With RFFE	AFFE	Ring+Little	Middle	Index	Thumb	—-	—-
S8	AFFE	Ring+Little	Thumb	Middle	—-	—-	—-
With RFFE	AFFE	Ring+Little	Thumb	Middle	AFFE	—-	—-
S9	AFFE	Thumb+Little	Index+Middle+Ring+Little	Thumb+Index	Thumb+Index	Index+Ring	—-
With RFFE	AFFE	Thumb+Little	Index+Middle+Ring+Little	Thumb,Index	—-	Index+Ring/Middle	—-
S10	AFFE	Thumb	Index	Middle	Little	——	—-
With RFFE	AFFE	—-	Index	Middle	Little	Thumb,Ring	—-

When moving along these independent latent dimensions from left to right as shown in Fig. 3.6b, muscle activations, corresponding to all the muscles, increase continuously. Monotonically increasing activation values for all the muscles indicate that these latent dimensions capture the overall variance of the sEMG data, instead of any task-specific variability. A video demonstration (Independent_LD.mp4) of change in activation values when moving along the independent latent dimension is provided in the supplementary material.

Muscle Synergies Coupled with Kinematic Synergies

Dimensions $\{9,10,11,12,13 \text{ and } 14\}$ represent the muscle synergies which are coupled with kinematic synergies. This coupling can be understood by the same procedure of sampling the latent points along one of the coupled dimension at a time and correlating it with both, the muscle activations and finger kinematics as shown in Fig. 3.7.

Fig. 3.7b shows the projection of latent space into dimensions $\{9 \text{ and } 10\}$ with the dotted blue line, along which the sampled latent points X_{samp} are mapped back to both the observational spaces by calculating the likelihoods $P(Y|X_{samp})$ and $P(Z|X_{samp})$. Reconstructed finger kinematics motion resemble with the all finger flexion-extension

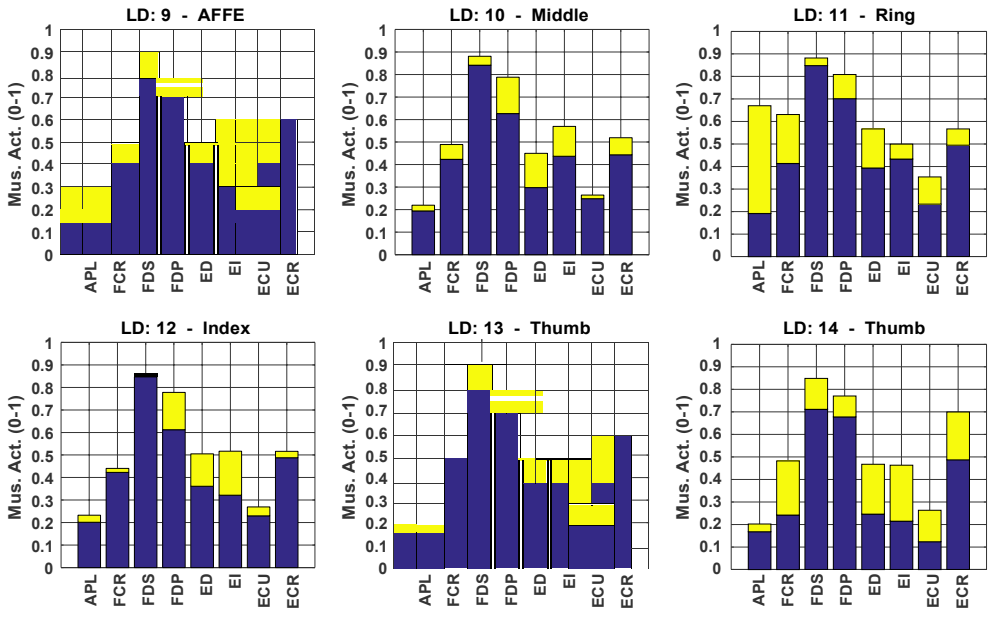

Figure 3.8: Shows the muscle activation values encoded in the shared latent dimensions $\{9,10,11,12,13,\text{and } 14\}$. Muscle activation values are obtained by following the same procedure of sampling latent points along a dimension. Yellow bars on the top of blue bars indicate the amount of modulation in the activation values with respect to the first point when moving along that dimension.

task. Visualization of the reconstructed muscle activation values and the corresponding finger kinematics at those six latent points which are indicated by the blue arrow in Fig. 3.7b are shown in Fig. 3.7a and 3.7c, respectively. Again the yellow bars on the top of blue bars in 3.7a indicate the amount of modulation in the activation values with respect to the first point when moving from left to right in Fig. 3.7b . Recovered finger motions corresponding to these coupled latent dimensions for all the subjects is presented in Table 3.2 while the muscle activation values for subject 1 (S1) are shown in Fig. 3.8.

Muscle activation values represented by coupled latent dimensions do not follow the trend of those represented by independent latent dimensions. In fact, moving along a coupled latent dimension, when resulting in the increase of activation values for some muscles, it results in the increase or decrease or no change in the activation values

corresponding to other muscles, and these variations are specific to a coupled latent dimension. This gives a notion that a coupled latent dimension encodes those activation values which are desired to achieve the finger kinematics represented by it. A video demonstration (Coupled_LD.mp4) of the generated muscle activations and related finger kinematics, when moving along the coupled latent dimensions are provided in the supplementary material.

It could be argued that the muscle synergy represented by a coupled latent dimension could be capturing the task-specific variability for a subject in contrast to the independent muscle synergy (dim. $\{1\}$) which is capturing the overall variance of the sEMG data. As coupled synergies are responsible for generating only a subset of values rather than large range of activation values (overall variance of the input sEMG), justifies the lower values of the ARD weights for the coupled muscle synergies (comparatively smaller blue bars for the dimensions 9,10,11,12,13, and 14) when compared with the higher ARD weight of an independent muscle synergy (blue bar for the dimension -1). A similar trend has also been observed in the remaining subjects.

It could be summarized from Fig. 3.4a and 3.5 that the variance presented in sEMG data from the eight muscles can be captured in the first two latent dimensions using a nonlinear approach. The independent muscle synergies (Dim. 1 and 2) in the both cases(EMG analyzed separately, and EMG analyzed together with finger kinematics), capture the overall variance of the sEMG data but shared synergies (coupled latent dimensions: $\{9,10,11,12,13$ and $14\}$) in latter case (EMG studied together with the kinematics) could be capturing the task-specific variability for a subject and responsible for generating only those activation values which are desired to achieve the kinematics represented by it. Please watch the attached video demonstration (Independent_LD.mp4, Coupled_LD.mp4) for further visualization.

3.4.3 Kinematic Estimation

The MRD model facilitates a way to interpret how different but related observation spaces interact with each other, by finding a shared latent space (X). In this study, the shared latent dimensions (muscle synergy coupled with finger kinematic synergy) represent the association of muscle activation with finger kinematics. The shared latent space provides us with a platform to visualize in the kinematic space, from what can be seen in the sEMG space within a fully probabilistic framework. Hence, the predicted

Table 3.3: The mean RMSE, Correlation Coefficient (ρ) and R-Square calculated between the estimated and original finger kinematics along with time required to predict a sample point.

Regression Methods	RMSE	Correlation coefficient(ρ)	R-Square	Time (in milliseconds)
Linear Regression on PCA Dimension	8.08± 1.28	0.50±0.08	0.31±0.13	0.000,09±0.000,1
Linear Regression on Full Dimension	7.66±1.22	0.57±0.07	0.38±0.12	0.000,43±0.000,10
NN on PCA Dimension	6.64±1.19	0.68±0.04	0.46±0.10	0.06±0.002
NN on Full Dimension	5.07 ± 0.90	0.82 ±0.04	0.68±0.07	0.09±0.010
Proposed Method	**3.4±0.89**	**0.91 ± 0.03**	**0.84± 0.05**	2.6 ± 0.79

NN - Neural Network, PCA - Principle Component Analysis.

point in the kinematic space gives a distribution instead of a point estimation, which makes the entire prediction process robust [48]. The finger kinematics is estimated from the shared latent space (X) by following the procedure presented in Algorithm 1.

Quality of the estimated finger kinematics using the proposed and other commonly used regression approaches have been evaluated on three metrics namely RMSE, R-square, and the Correlation Coefficient (ρ) as shown in Table 3.3. The estimated marker positions follow the measured values with an average correlation of 0.91 ± 0.03, R-square of 0.84 ± 0.05 and the RMSE of 3.44 ± 0.87, respectively, which show the best results when compared with other regression methods. Subject wise RMSE corresponding to all the five methods have been shown in Fig. 3.9.

Statistical significance was evaluated using one-way Annova on three evaluation metrics namely Correlation Coefficient, R-square and Root Mean Square Error (RMSE) as dependent or response variable to determine if the accuracy of estimated finger kinematics were significantly improved using MRD model when compared with other commonly used regression approaches. There are five different regression approaches (independent variable) namely LR trained on reduced dimensions (LR-PCA), Linear Regression using full dimension (LR-Full), Neural Network (NN) on reduced dimensions (NN-PCA), NN on full dimensions (NN-FULL) and proposed method the MRD model. It can be seen from Fig. 3.11a, 3.11b and 3.11c that MRD has statistically significant improvement ($p \leq 0.0001$) in the prediction accuracies over other regression approaches.

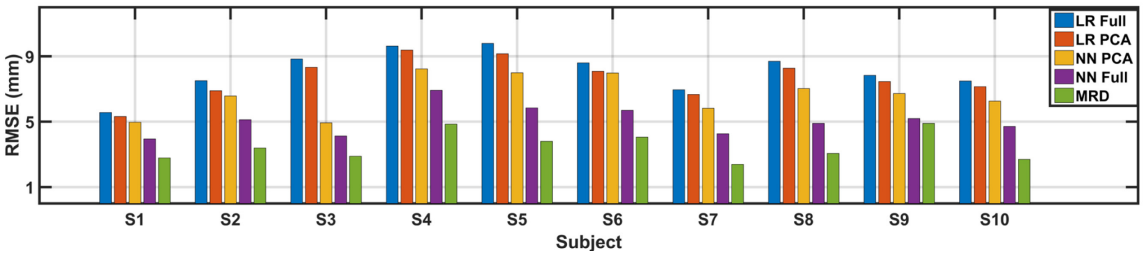

Figure 3.9: Root Mean Square Error (RMSE) calculated between the measured and estimated 3D coordinate corresponding to 23 marker positions in the hand for all 10 subjects corresponding to all the five methods.

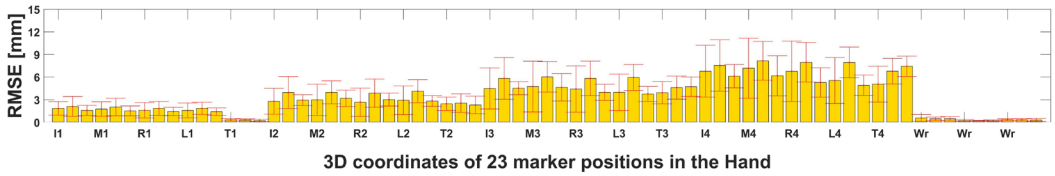

Figure 3.10: Multi-fingered kinematics estimation performance over 10 subjects across all three sets of tasks using the MRD model, showing the Root Mean Square Error (RMSE) calculated between the measured and estimated 3D coordinates corresponding to 23 marker positions in the hand, respectively. The x-axis letter labels represent the index, middle, ring, little and thumb, while the numbers 1,2,3 and 4 are the MCP, PIP, DIP, and tip for the fingers, and CMC, MCP, PIP, and tip marker positions for the thumb, respectively. The x-axis label, Wr, in the figure, referring to the three markers used in the wrist. Error bars in the red shows the standard deviation across the subjects.

3.5. Discussion

This paper showed that there exists an association between finger kinematics and muscle activations, manifested in coupled muscle synergies, by jointly studying the two related spaces through multi-view learning. This study also demonstrated how the proportional and simultaneous estimation of finger kinematics can be achieved by making use of the shared variance between the Muscle Activation space (Y) and the Kinematic space (Z) in a probabilistic framework.

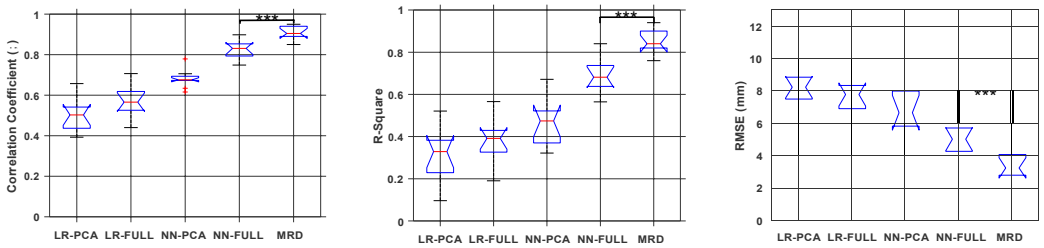

(a) (b) (c)

Figure 3.11: Comparison of estimation performance between MRD and other commonly used regression approaches. Evaluation on three metrics: (a) Correlation (b) R-square and (c) Root Mean Square Error (RMSE). *** indicates $p \leq 0.0001$ for one-way Annova.

3.5.1 Nonlinear Kinematic Synergies

Table 3.2 shows the reconstructed finger kinematics when the dimensions representing kinematic synergies in the shared latent space (X) were explored. Dimension 9 consistently encodes the kinematic information of the All Finger Flexion-Extension (AFFE) task even across different subjects. This can be attributed that dimension 9 captures a larger variance of kinematic data from this task, nearly 20 markers' positions varying as compared to only 5 to 6 markers' position changing at a time in the Individual Finger Flexion-Extension (IFFE) task.

The kinematics of the thumb, on the other hand, is encoded in a separate dimension. This highly independent motion of the thumb is captured in most of the subjects (8 out of 10). While, coupled motion of the thumb with other fingers is captured in the other dimensions. From the kinematics point of view, this is likely due to the opposite direction of the thumb as compared with motions of the other fingers. The thumb also has more degrees-of-freedom (DOFs) and has more independent movements compared to the rest of the other fingers.

The kinematics of the individual finger's movement are inconsistently encoded in different dimensions 10-13 across subjects. Some dimensions contain only the data variance of individual finger exclusively, while others contain the variance of individual finger movements coupled with other finger's movements. This natural coupling of finger movements is also summarized in Table 3.2, which describes the anatomical and kinesiological similarities of the targeted muscles to control similar fingers.

The synergies obtained by our method captures these anatomical couplings quite well, with couplings that occur between adjacent fingers, for example Index-Middle-Ring, rather than with distant fingers Index-Little. These result consistently showed that the extracted muscle synergies are congruent with the hand physiology.

The nonlinear kinematic synergies have also been analyzed for the models trained with including the random finger flexion-extension task. Extracted kinematics for some coupled latent dimensions in some subjects, however, has been changed, but similar observations can be observed in Table 3.2 with RFFE task as well.

The finger kinematics and the sEMG signals are highly nonlinear in nature, and therefore an algorithm that can cope with nonlinearities is better suited for their analysis. Thus extracting nonlinear muscle and kinematic synergies, using the MRD model, and its effectiveness in reconstructing the related higher dimensional spaces and accurately predicting finger kinematics justifies its use. From the best of our knowledge, this is the first sEMG study to introduce a factorized latent model to nonlinearly extract the muscle synergies with relevant weights associated with each synergy, which explains its importance in the related spaces.

3.5.2 Estimation of Finger Kinematics

The experimental results in the previous section show that the MRD model with the automatic dimensionality determination of the latent spaces is an effective model for learning the correlations that exist between the muscle activations and the finger kinematics. Although the dimensions are highly redundant in the kinematic space, the proposed model is able to reconstruct back as large as 69 dimensions $(23 \times 3 = 69)$ on the hand skeleton model.

The choice of operating in the output joint marker space was to induce high dimensionality in the output space and to show that the model is capable of dealing with high dimensional data very well. One other advantage of the proposed method is that it can learn corresponding latent space manifolds from any data representation or output spaces, such as joint velocity or joint torque and stiffness space [49]. Operating in these spaces is particularly useful since these can be explicitly used as direct control signals for robotic devices.

One advantage of using the proposed shared synergistic model is its ability to consider nonlinear mappings using GPs with an ARD covariance function shown in (5).

This gives a data-driven approach to address the compact representation of both the sEMG and high-DOF finger kinematics.

3.5.3 Implementation and limitations

This study is limited to offline analysis with data from healthy and able-bodied subjects to test the feasibility of our approach. Though this can be used as an initial benchmark, for future implementations, further verification and validation has to be done for training different models using data from amputees or subjects with hand impairments. A good candidate for this is to use large sEMG and motion datasets obtained from both healthy and impaired subjects such as those provided by the Ninapro database [50].

In practice, it is desirable for the controller to use as little calibration data as possible and should generalize to movements for which exhaustive training data is not available [1]. Most of the computational time (99%) is due to the training of the MRD model. The typical computational complexity of a sparse implementation of the MRD model is $O(Nm^2)$, where N is the number of data sample used, and m is the number of inducing points. This can be quite prohibitive with many sEMG applications where re-calibration is done to adapt to the time-varying nature of sEMG.

Chapter 4

An Approach to Extract Nonlinear Muscle Synergies from sEMG through Multi-Model Learning

How does the Central Nervous System (CNS) controls a group of muscles is an important question in the field of motor control. A common conception is developed over the years that the CNS make use of predefined activation patterns, known as muscle synergies during task execution. These muscle synergies are extracted by applying any of the factorization algorithms such as Non-Negative Matrix Factorization (NNMF), Independent Component Analysis (ICA) or Principle Component Analysis (PCA) on a concatenated surface EMG data set recorded from the target muscles. However, the step to concatenate sEMG signals before they are given as input to these linear algorithm is crucial as the synergistic structure changes significantly based on the number and choice of muscles considered during concatenation step. To address this problem, we propose a new approach of extracting muscle synergies by treating sEMG signals from each muscle as an individual view and then learning the synergistic structure among them if it exists using multi-view learning. In this study, we propose to use Manifold Relevance Determination (MRD) to find nonlinear synergies from sEMG by assuming the sEMG of a muscle as an individual view. Results have shown that synergistic patterns extracted using our approach are consistent upon addition of sEMG signals from new muscles.

4.1. Introduction

Motor tasks are generated when certain group of muscles activated in some coordination by the central nervous system (CNS). But how does the CNS generate the control signals for such large and complex muscular system to achieve a wide variety of tasks? The idea that CNS does not control each and every muscle independently instead group of muscles are controlled through some predefined patterns termed as muscle synergies, developed over the years [51].

To extract these synergistic structures, surface electromyography (sEMG) data is recorded by placing the number of electrodes on the target muscles while user perform the desired task set. Concatenated sEMG data corresponding to all muscles as a whole is then given as input to any linear or nonlinear factorization or dimensionality reduction algorithms such as non-negative matrix factorization (NNMF), independent component analysis (ICA) or principle component analysis (PCA). All of these are most commonly used and established methods in the literature. However, in a study by M. Spuler et al. [26], it has been shown that these algorithms failed to represent agonist-antagonist muscle relationships in the extracted synergies due to their linear nature while autoencoder (non-linear approach) have successfully represented it.

Other than the linear nature of these algorithms, Steele et al. [30] have shown that the step to concatenate sEMG signals before they are given as input to the algorithm is crucial, as the synergistic structure changes significantly based on the number and choice of muscles during the concatenation step, also demonstrated, later in this study. The quality and quantity of such synergistic patterns are decided, based on their ability to reconstruct original signals, which in turn themselves can be contaminated or may not be the actual representation of electrical activity took place in muscles during task execution as such experiments are generally based on surface sEMG [6].

In this study, we propose a new approach of extracting muscle synergies with an initial assumption that CNS is controlling every muscle individually and hence sEMG of each muscle should be treated as a separate view. However, if a group of muscle is controlled together through some underlying synergistic patterns then such co-activation should be reflected in a shared latent space, learned, corresponding to all modalities (muscles).

We propose to use Manifold Relevance Determination (MRD) model [31] for learning any correlation if it exists among a group of muscles by learning a shared low di-

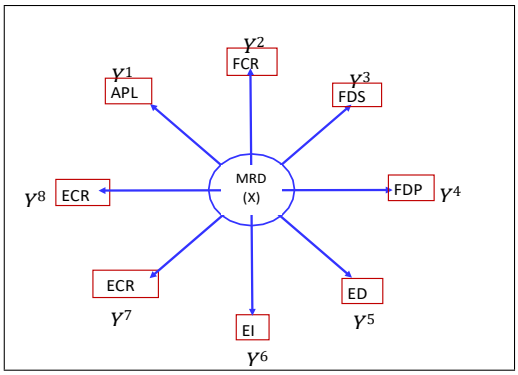

Figure 4.1: Schematic overview of proposed method for extracting muscle synergies using Manifold Relevance Determination (MRD) model. Muscle activations corresponding to the eight muscles of the forearm which are known to contribute finger movements are given as eight separate modalities ($Y^1, Y^2, \ldots, Y^8$) to the MRD model as input. MRD learns a shared latent space (X) which explains the relationship or co-activation among muscles when subject was performing individual and all finger flexion-extension task.

mensional space. The MRD model is an example of multi-view learning where data from different but related sources are studied together as the data from one source can not comprehensively describe the whole phenomenon [52]. Learning from multimodal sources offers the possibility of capturing correspondences between modalities and gaining an in-depth understanding of natural phenomena [53].

MRD models the relationship between M modalities through a common latent space (X). The MRD model can be understood as an extension of Shared Gaussian Process Latent Variable Model (SGPLVM) [54] with an approximate Bayesian inference which allows the use of a more complex covariance function to determine the relevance of every dimension in the latent space automatically.

4.2. Methods

In this section, we present the MRD model [31] and its formulation, used for finding the shared latent space from M modalities of the data.

4.2.1 Manifold Relevance Determination (MRD)

MRD is an example of multi-modal learning in which factorization of the nonlinear latent space is learned from multiple modalities of the data. Damianou et al. [31, 55] have presented the model formulation and experiment analysis of shared latent space for the two modalities, however it can easily be extended to the M modalities of the data. The problem is formulated as follows: Given that we have observation data from M different modalities, each containing N samples $Y^m \in \mathbb{R}^{N \times D_m}$ where $m \in M$, the goal of the model is to find a shared latent variable parameterization in a space $X \in \mathbb{R}^{N \times Q}$, ($Q << D_m$), that relates corresponding pairs of observations from M modalities. It is assumed that the each view is generated from a low dimensional manifold mapped from smooth functions $\{f_d^m\}_{d=1}^{D_m} : X \rightarrow Y^m$, corrupted by noise:

$$
\begin{aligned}
y_{id}^1 &= f_d^{Y^1}(\mathbf{x}_i) + \varepsilon_{id}^{Y^1} \\
y_{id}^2 &= f_d^{Y^2}(\mathbf{x}_i) + \varepsilon_{id}^{Y^2} \\
&\ddots \\
y_{id}^M &= f_d^{Y^M}(\mathbf{x}_i) + \varepsilon_{id}^{Y^M}
\end{aligned}
$$

where $\{y^m\}_{id}$ represents dimension d of sample point i and $\varepsilon_{id}^{Y^m}$ are sampled from a zero mean Gaussian distribution for the view m. This leads to the likelihood under the model, $P(Y^1, Y^2, \ldots, Y^M | X, \vartheta)$, where $\vartheta = \{\vartheta^{Y^1}, \vartheta^{Y^2}, \ldots, \vartheta^{Y^M}\}$ contains the parameters of the mapping functions and noise variances. Finding the latent representation X and mapping functions $f^1, f^2, \ldots, f^M$ is an ill-constrained problem. Lawrence provided a solution by placing GP priors over the mapping and the resulting model is the Gaussian Process Latent Variable Model (GPLVM) framework [33]. In this framework, each generative mapping is modeled as a product of independent Gaussian processes (GP's) parametrized by the kernel or covariance function $K = \{K^1, K^2, \ldots, K^M\}$ evaluated over the latent variable X, so that

$$
P(F^1 | X, \vartheta^1) = \prod_{d=1}^{D_1} N(f_d^1 | \mathbf{0}, K^1)
$$

$$P(F^2|X,\vartheta^2) = \prod_{d=1}^{D_2} N(f_d^2|\mathbf{0},K^2)$$

$$\ddots$$

$$P(F^M|X,\vartheta^M) = \prod_{d=1}^{D_M} N(f_d^M|\mathbf{0},K^M)$$

where $F^1 = \{f_d^1\}_{d=1}^{D_1}$ with $f_{id}^1 = f_d^1(\mathbf{x}_i)$ and similarly for other M modalities. This allows the general nonlinear mapping function F to be marginalized out leading to a likelihood function in the form of a product of Gaussian densities:

$$P(Y^1,Y^2,..Y^M|X,\vartheta) = \prod_{M=\{Y^1,Y^2,...,Y^M\}} \int p(M|F^M)p(F^M|X,\vartheta^M)dF^M \quad (4.1)$$

Integration over (1) is then done by variationally marginalizing out X by using variational approximation techniques used for standard GPLVMs. A non-standard but analytical solution through variational learning techniques and using induced variables is described in [31, 36, 37]. The shared latent space (X) is composed of private subspaces corresponding to each view, representing the private variance for each view ($X = X^1, X^2, \ldots, X^M$) and shared subspaces, representing the shared variances among the modalities ($X = X^S, S \subseteq 1,2,\ldots,M$). Bayesian training automatically allocates the dimension of this shared latent space (X) using automatic relevance determination (ARD) priors [31].

4.3. Datasets

For this study, we used a publicly available dataset [56]. In this dataset, surface EMG signals were extracted from 8 extrinsic muscles of the hand using bipolar active-type Ag-AgCl electrodes, with inter-electrode distance of 20 mm, were placed on the following extrinsic muscles in the forearm: Abductor Pollicis Longus(APL), Flexor Carpi Radialis(FCR), Flexor Digitorum Superficialis(FDS), Flexor Digitorum Profundus(FDS), Extensor Digitorium(ED), Extensor Indices(EI), Extensor Carpi Ulnaris(ECU) and Extensor Carpi Radialis(ECR). The sEMG signals were measured using a compact

BA1104 pre-amplifier and a TU-4 telemetry unit (Digitex Lab. Co. Ltd). Each participant, seated with their dominant hand and elbow comfortably positioned on a flat surface table, were asked to do different flexion and extension finger movement tasks which include the (i) individual finger flexion-extension and (ii) flexion-extension of all fingers. Five trials of each task were recorded where in a trial every task was repeated for 20 seconds. All the trails were recorded sequentially. And participants were allowed to take rest anytime during the experiment. All raw sEMG signal were first preprocessed which include rectification, normalization, and low pass filtered (4Hzcut-off frequency). After sEMG signals were converted into muscle activations using the model proposed by Buchanan et al. [43]. The total data used included those of 5 healthy and intact participants (4 Male, 1 Female, aged 26-31 years old). Dataset from subject 1 is used for visualization of the results from NNMF and MRD.

4.4. Results and Discussion

This section first describes the synergies extracted using NNMF and their limitation, then the synergies discovered using the MRD model are presented and explained. In the last, it has been demonstrated that the synergies extracted using the MRD model are consistent upon addition of sEMG data corresponding to new muscles.

4.4.1 Synergies Extracted Using NNMF

Synergies are extracted using NNMF from the data obtained after concatenation of muscle activations corresponding to the first six ($Y^1, Y^2, \ldots, Y^6$) and then all eight muscles ($Y^1, Y^2, \ldots, Y^8$) as shown in Fig. 4.2a and 4.2b, respectively. The number of synergies is decided based on standard criteria of Variance Accounted For metric ($VAF \geq 90\%$). Synergies extracted in Fig. 4.2a should be retained in the synergies obtained upon addition of sEMG from two more muscles, in Fig. 4.2b, with some added activation corresponding to the newly added muscles as and if predefined patterns are used to control the muscles during task execution, according to muscle synergy hypothesis. And it is reflected to an extent for muscle synergies 1 and 2 (if we ignore APL and EI activation in synergy 1 while ED activation in synergy 2). However, it is hard to relate the muscle synergies 3, 4 and 5 from Fig. 4.2a to the muscle synergies

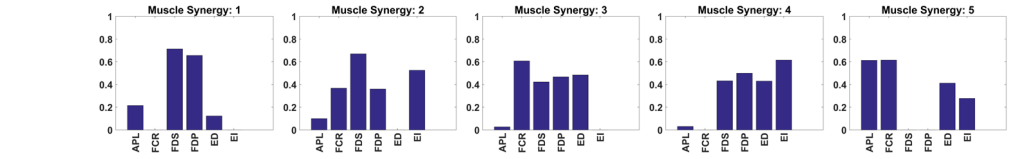

(a)

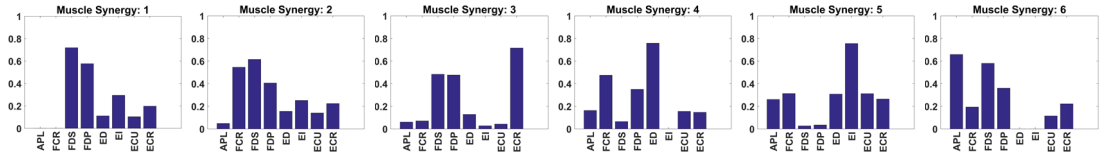

(b)

Figure 4.2: Shows the muscle synergies extracted using NNMF from the sEMG of subject 1. (a) shows the extracted muscle synergies from the dataset obtained after the concatenation of first six muscles while (b) shows the extracted muscle synergies for all eight muscles. In both the cases no. of synergies are decided based on the VAF metric ($VAF \geq 90\%$). Synergies shown in (b) should retain the co-activation of muscles learned in (a), with some added activation or new patterns corresponding to the new muscles as and if predefined patterns are used to control the muscles during task execution, according to muscle synergy hypothesis. And it is reflected till a extent for muscle synergies 1 and 2. However, it is hard to relate the muscle synergies 3, 4 and 5 from Fig. 4.2a to the muscle synergies shown in Fig. 4.2b because the algorithm comes up with some new co-activation patterns.

shown in Fig. 4.2b because the algorithm comes up with some new co-activation patterns. Based on this result it can be argued that the addition of sEMG signals from new muscles influences the synergistic structure significantly extracted using NNMF [30]. And it is difficult to measure electrical activities for all the muscles, CNS controls during a task, at least, in the multi-fingered movement for the dexterous manipulation of objects, to find out which set of the pattern might be the actual because originals are never known. Results, shown in this section suggest that the approach to extract synergies should be reconsidered and need to be redefined.

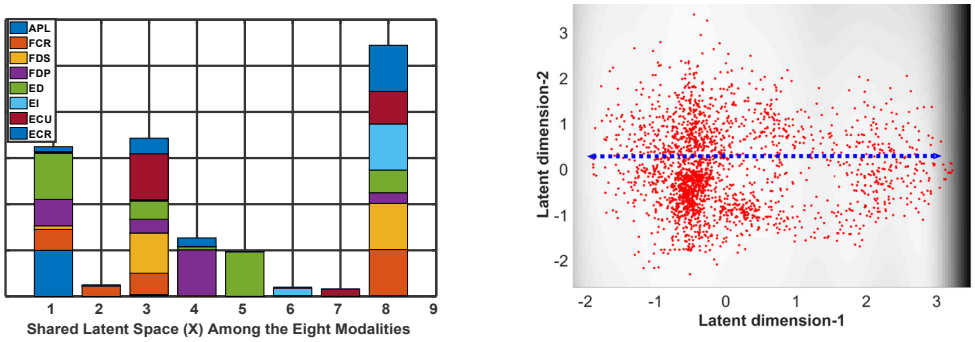

(a) (b)

Figure 4.3: The Shared latent space obtained among the eight muscles (a) shows the scaled ARD weight corresponding to all eight modalities. For easy interpretation, they are depicted in the form of stacked bars. A dimension is shared in the latent space when the same latent dimensions corresponding to two or more views are active. Every shared dimension in the latent space represents a muscle synergy. (b) shows the 2D projection of shared latent space X into latent dimension$\{1$ and $2\}$. Muscle activation values corresponding to the latent dimensions can be obtained by varying the latent points along it as shown by the dotted blue line in (b), while keeping the points fixed on the other dimensions.

4.4.2 Synergies Extracted Using MRD

To discover the synergistic patterns among the muscles group, muscle activation corresponding to each muscle is treated as an individual view, and hence eight modalities corresponding to eight channel sEMG are analyzed together in the MRD model. Interaction among the various modalities can be visualized through the shared latent space in the MRD model. Initially, the dimensionality of the shared latent space can be set to eight or more. Setting the larger value for latent dimensions in the beginning will not force the model to show correspondence among modalities when it does not exist while ARD kernel will automatically turn off a latent dimension when it has no or very little significance in reconstructing the higher dimensional spaces.

Fig. 4.3a shows the shared latent space obtained using the MRD model while Fig. 4.3b shows the 2D projection of shared latent space into dimensions $\{1$ and $2\}$. The red dots in Fig. 4.3b represents the posterior mean of each training data point, while

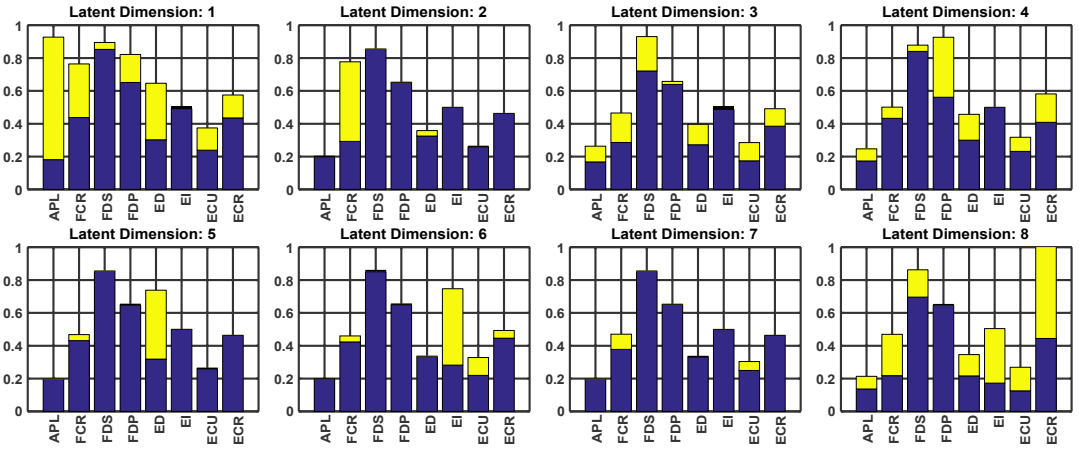

(a)

Figure 4.4: Visualization of muscle activation values corresponding to all active latent dimensions as shown in the 4.3a. Yellow bars on the top of blue bars indicate the amount of modulation in the activation values with respect to the first point when moving from left to right in 4.3b.

gradient of the background represents posterior variance which signifies the confidence of the model in projecting the corresponding point in higher dimensional space (high confidence for the white region while the low for the black region).

A dimension in the shared latent space represents a muscle synergy. Stacked bars in a latent dimension represents the co-activation of concerned muscles while length of a bar signifies the amount of modulation in the activation values with respect to each other. To understand the shared information (co-activation) encoded in each latent dimension clearly, higher dimensional space (sEMG) corresponding to each view (muscle) are reconstructed back by varying the latent points along a dimension while keeping the latent points fixed corresponding to other latent dimensions as shown in Fig. 4.3b by a dotted blue line.

The reconstructed sEMG of all eight muscles corresponding to all latent dimensions are shown in Fig. 4.4a. Where blue bars represent the activation values corresponding to the left most point in the dotted blue line in Fig. 4.3b while yellow bars on the top of blue bars are representing the change in the activation values as moving from left to right along that line. The yellow bars are the actual representation of

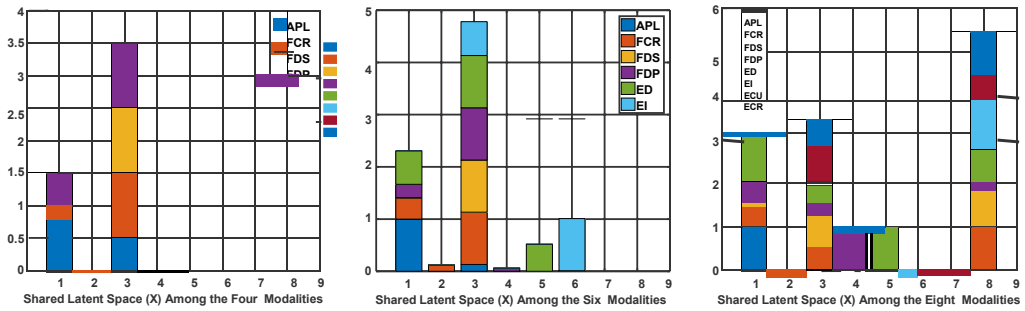

(a) (b) (c)

Figure 4.5: Shows the comparison of synergies learned with the sEMG dataset corresponding to the (a) four (b) six and (c) eight muscles for Subject 1. Learned co-activation with fewer muscles are retained upon addition of more muscles as can be observed by matching the stacked bars corresponding to the muscles.

co-activation which is encoded in the latent dimensions. It is worth noting that the synergies obtained using MRD are not directly comparable with the synergies extracted using traditional algorithms such as NNMF, PCA or Autoencoder. Latent dimension 1 in Fig. 4.3a can be interpreted as synergy representing the co-activation of almost all muscles except the FDS and EI with the large range of variation in the activation values for the APL muscle (long bar) with respect to the variation in the activation values for other muscles, as can be observed in reconstructed muscle activations corresponding to the latent dimension 1 in Fig. 4.4a in yellow bars.

Consistency of the Extracted Synergistic Patterns using MRD

To ensure that the synergistic structures extracted through the approach of considering sEMG from each muscle as an individual view is not affected by addition of sEMG signals from other muscles, separate set of MRD Models were trained with four and six individual modalities corresponding to sEMG of first four and six muscles for every subject. Shared latent space corresponding to four, six, and eight modalities for subject 1 are shown in Fig. 4.5a, 4.5b and 4.5c, respectively. It can be observed in the three shared latent spaces that coupling among muscles detected with fewer muscles is retained upon addition of more muscles. Latent dimension 1 in Fig. 4.5a, shows the coupling of APL, FCR and FDP which can also be observed in the latent dimension 1

of Fig.4.5b with an added co-activation of ED and in Fig. 4.5c with a negligible or a little co-activation with respect to the muscles FDS and ECU. A similar trend has also been observed for other four subjects used in this study.

Chapter 5

Conclusion and Future Work

5.1. Conclusion

This study has focused on exploring the relationship between the EMG and kinematics space and come up with an approach to mitigate the drawbacks of linear algorithms. In chapter 3 two different but related nonlinear spaces the EMG and the Kinematics have been analyzed independently and jointly in the shared low dimensional space. We have found out that the studying EMG together with the kinematics, an association between the two spaces can be discovered in low dimensional space. Further analysis of this learned association reveals that each muscle synergy (a latent dimension) which is shared with the kinematic synergies could be capturing the task-specific variations and can be utilized for estimating the kinematics from the EMG signal for proportional myoelectric control.

This study has further shown the application of such extracted nonlinear synergies and the discovered association between muscle and kinematics synergies for estimating the finger kinematics using the nearest neighbor approach and the inference algorithm presented in chapter 3. The proposed approach has outperformed other standard linear and nonlinear regression techniques in the kinematics estimation from the muscle activations.

In the later part of this study, we have focused on proposing an approach to extract the synergistic patterns which are consistent over the addition of EMG signals from new muscles. As previous studies have shown how the number and choice of muscles affect the extracted synergistic patterns from the most popular Non-Negative

Matrix Factorization (NNMF) algorithm. Chapter 4 has presented the use of the MRD model, and shown that the extracted nonlinear muscle synergies (co-activation of muscles) with fewer muscles, retained, over the addition of sEMG data from new muscles, which suggest that the proposed approach has potential to extract consistent synergistic patterns from the surface electromyography.

As a conclusion, the findings of Chapter 3 presents a viable solution for accurate and intuitive myoelectric control for handling high DOFs in robotic hand prosthesis while Chapter 4 presents a new approach to extract muscle synergies, for the motor control community by removing the drawbacks of existing linear synergy extraction algorithms such as NNMF.

5.2. Future Work

For future work, the approach presented in chapter 3 can be used to understand the neural implementation of muscle synergies by simultaneously recording neural and muscle activities when performing different motor tasks [57–60]. The existence of the shared part in the latent space supports the muscle synergy hypothesis and the method for extracting muscle synergies from sEMG signals. This work can be further extended by including task-related variables for understanding the relationship among these three different but related observational spaces.

Training the MRD model is a computationally expensive task, and retraining of the model is needed frequently due to the time-varying nature of sEMG. For the clinical application, the use of the MRD model may not be an appropriate choice, and exploration of some time-efficient multiview learning algorithms such as presented in [61] is one of the crucial future work of this study.

The approach presented in chapter 4 can further be extended to predict muscle activation values for a large group of muscles from the small group of muscles by making use of learned non-linear correlation among muscles to reduce the number of electrodes required for mapping accurate kinematics as discussed in [62].

Acknowledgements

First of all, I would like to express my sincerest gratitude to my supervisor, Professor Tomohiro Shibata, who without any reservations, continuously guided and supported me. This work would not have been possible without him. He welcomed and took me under his guidance. His generosity has allowed me to complete my studies in Japan. He is more than my adviser and mentor, I will be forever grateful for his dedication to his students. His words and encouragement have always inspired and brought out the very best in us.

Besides my supervisor, I would like to thank the rest of my dissertation committee members: Professor Tetsuo Furukawa, Professor Keiichi Horio, and Associate Professor Tomoya Tamei for generously offering their time, great support and invaluable advice to shape my final dissertation.

In the completion of this work, many people have helped me along the way. I would like to thank Dr. Jimson Ngeo, Dr. Nishanth Koganti, Vishal Gaurav, Shinta Hara and Tsuyoshi Shibata for their valuable insights and contributions.

Finally, I would like to thank the Japan Government MEXT Scholarship Program and the Grant-in-Aid for Scientific Research from Japan Society for the Promotion of Science, for the support in my education and research. Without them, my dream of studying in Japan would never have come true. Thank you for the valuable opportunity.

References

[1] J. Hahne, F. Biebmann, N. Jiang, H. Rehbaum, D. Farina, F. Meinecke, K.-R. Muller, and L. Parra, "Linear and nonlinear regression techniques for simultaneous and proportional myoelectric control," *IEEE Trans. on Neural Syst. and Rehabil. Eng.*, vol. 22, no. 2, pp. 269–279, March 2014.

[2] D. Farina, N. Jiang, H. Rehbaum, A. Holobar, B. Graimann, H. Dietl, and O. Aszmann, "The extraction of neural information from the surface EMG for the control of upper-limb prostheses: Emerging avenues and challenges," *IEEE Trans. on Neural Syst. and Rehabil. Eng.*, vol. 22, no. 4, pp. 797–809, 2014.

[3] Y. Huang, K. B. Englehart, B. Hudgins, and A. D. Chan, "A gaussian mixture model based classification scheme for myoelectric control of powered upper limb prostheses," *IEEE Trans. on Biomedical Eng.*, vol. 52, no. 11, pp. 1801–1811, 2005.

[4] A. J. Young, L. H. Smith, E. J. Rouse, and L. J. Hargrove, "Classification of simultaneous movements using surface EMG pattern recognition," *IEEE Trans. on Biomedical Eng.*, vol. 60, pp. 1250–1258, 2013.

[5] N. Jiang, H. Rehbaum, I. Vujaklija, B. Graimann, and D. Farina, "Intuitive, online, simultaneous, and proportional myoelectric control over two degrees-of-freedom in upper limb amputees," *IEEE Trans. on Neural Syst. and Rehabil. Eng.*, vol. 22, no. 3, pp. 501–510, 2014.

[6] M. Ison and P. Artemiadis, "The role of muscle synergies in myoelectric control: trends and challenges for simultaneous multifunction control," *Journal of Neural Engineering*, vol. 11, no. 5, p. 051001, 2014.

[7] N. Jiang, S. Dosen, K.-R. Müller, and D. Farina, "Myoelectric control of artificial limbs–is there a need to change focus," *IEEE Signal Process. Mag*, vol. 29, no. 5, pp. 152–150, 2012.

[8] V. Kumar, Y. Tassa, T. Erez, and E. Todorov, "Real-time behaviour synthesis for dynamic hand-manipulation," in *IEEE Int. Conf. on Robotics and Automation (ICRA)*. IEEE, 2014, pp. 6808–6815.

[9] A. d'Avella, P. Saltiel, and E. Bizzi, "Combinations of muscle synergies in the construction of a natural motor behavior," *Nature neuroscience*, vol. 6, no. 3, pp. 300–308, 2003.

[10] J. Romero, T. Feix, C. H. Ek, H. Kjellstrom, and D. Kragic, "Extracting postural synergies for robotic grasping," *IEEE Trans. on Robotics*, vol. 29, no. 6, pp. 1342–1352, 2013.

[11] I. V. Grinyagin, E. V. Biryukova, and M. A. Maier, "Kinematic and dynamic synergies of human precision-grip movements," *Journal of neurophysiology*, vol. 94, no. 4, pp. 2284–2294, 2005.

[12] M. Santello, M. Flanders, and J. F. Soechting, "Postural hand synergies for tool use," *The Journal of Neuroscience*, vol. 18, no. 23, pp. 10 105–10 115, 1998.

[13] A. d'Avella, A. Portone, L. Fernandez, and F. Lacquaniti, "Control of fast-reaching movements by muscle synergy combinations," *The Journal of neuroscience*, vol. 26, no. 30, pp. 7791–7810, 2006.

[14] L. H. Ting, "Dimensional reduction in sensorimotor systems: a framework for understanding muscle coordination of posture," *Progress in brain research*, vol. 165, pp. 299–321, 2007.

[15] M. Tagliabue, A. Ciancio, T. Brochier, S. Eskiizmirliler, and M. Maier, "Differences between kinematic synergies and muscle synergies during two-digit grasping," *Frontiers in human neuroscience*, vol. 9, 2015.

[16] N. Jiang, K. B. Englehart, and P. A. Parker, "Extracting simultaneous and proportional neural control information for multiple-dof prostheses from the surface electromyographic signal," *IEEE Transactions on Biomedical Eng.*, vol. 56, no. 4, pp. 1070–1080, 2009.

[17] P. K. Artemiadis and K. J. Kyriakopoulos, "Emg-based control of a robot arm using low-dimensional embeddings," *IEEE Transactions on Robotics*, vol. 26, no. 2, pp. 393–398, 2010.

[18] N. Jiang, I. Vujaklija, H. Rehbaum, B. Graimann, and D. Farina, "Is accurate mapping of EMG signals on kinematics needed for precise online myoelectric

control?" *IEEE Trans. on Neural Syst. and Rehabil. Eng.*, vol. 22, no. 3, pp. 549–558, May 2014.

[19] J. Ma, N. V. Thakor, and F. Matsuno, "Hand and wrist movement control of myoelectric prosthesis based on synergy," *IEEE Transactions on Human-Machine Systems*, vol. 45, no. 1, pp. 74–83, 2015.

[20] S. Zhang, X. Zhang, S. Cao, X. Gao, X. Chen, and P. Zhou, "Myoelectric pattern recognition based on muscle synergies for simultaneous control of dexterous finger movements," *IEEE Transactions on Human-Machine Systems*, vol. 47, no. 4, pp. 576–582, 2017.

[21] C. Lin, B. Wang, N. Jiang, and D. Farina, "Robust extraction of basis functions for simultaneous and proportional myoelectric control via sparse non-negative matrix factorization," *Journal of neural engineering*, 2017.

[22] S. Muceli, N. Jiang, and D. Farina, "Extracting signals robust to electrode number and shift for online simultaneous and proportional myoelectric control by factorization algorithms," *IEEE Trans. on Neural Syst. and Rehabil. Eng.*, vol. 22, no. 3, pp. 623–633, 2014.

[23] C. Alessandro, I. Delis, F. Nori, S. Panzeri, and B. Berret, "Muscle synergies in neuroscience and robotics: from input-space to task-space perspectives," *Frontiers in computational neuroscience*, vol. 7, p. 43, 2013.

[24] S. A. Chvatal, G. Torres-Oviedo, S. A. Safavynia, and L. H. Ting, "Common muscle synergies for control of center of mass and force in nonstepping and stepping postural behaviors," *Journal of neurophysiology*, vol. 106, no. 2, pp. 999–1015, 2011.

[25] L. H. Ting and J. M. Macpherson, "A limited set of muscle synergies for force control during a postural task," *Journal of neurophysiology*, vol. 93, no. 1, pp. 609–613, 2005.

[26] M. Spüler, N. Irastorza-Landa, A. Sarasola-Sanz, and A. Ramos-Murguialday, "Extracting muscle synergy patterns from emg data using autoencoders," in *International Conference on Artificial Neural Networks*. Springer, 2016, pp. 47–54.

[27] I. Delis, B. Berret, T. Pozzo, and S. Panzeri, “Quantitative evaluation of muscle synergy models: a single-trial task decoding approach,” *Frontiers in computational neuroscience*, vol. 7, p. 8, 2013.

[28] M. C. Tresch, V. C. Cheung, and A. d’Avella, “Matrix factorization algorithms for the identification of muscle synergies: evaluation on simulated and experimental data sets,” *Journal of neurophysiology*, vol. 95, no. 4, pp. 2199–2212, 2006.

[29] N. Lambert-Shirzad and H. M. Van der Loos, “On identifying kinematic and muscle synergies: a comparison of matrix factorization methods using experimental data from the healthy population,” *Journal of neurophysiology*, vol. 117, no. 1, pp. 290–302, 2016.

[30] K. M. Steele, M. C. Tresch, and E. J. Perreault, “The number and choice of muscles impact the results of muscle synergy analyses,” *Frontiers in computational neuroscience*, vol. 7, p. 105, 2013.

[31] A. Damianou, C. Ek, M. Titsias, and N. Lawrence, “Manifold relevance determination,” *arXiv preprint arXiv:1206.4610*, 2012.

[32] C. Rasmussen and C. Williams, *Gaussian processes for machine learning*. MIT Press, Cambridge, MA, USA, 2006.

[33] N. Lawrence, “Probabilistic non-linear principal component analysis with gaussian process latent variable models,” *The Journal of Machine Learning Research*, vol. 6, pp. 1783–1816, 2005.

[34] A. Shon, K. Grochow, A. Hertzmann, and R. P. Rao, “Learning shared latent structure for image synthesis and robotic imitation,” in *Advances in Neural Information Processing Systems*, 2005, pp. 1233–1240.

[35] C. H. Ek, J. Rihan, P. H. Torr, G. Rogez, and N. D. Lawrence, “Ambiguity modeling in latent spaces,” in *Machine Learning for Multimodal Interaction*. Springer, 2008, pp. 62–73.

[36] M. K. Titsias and N. D. Lawrence, “Bayesian gaussian process latent variable model,” in *International Conference on Artificial Intelligence and Statistics*, 2010, pp. 844–851.

[37] A. Damianou, M. K. Titsias, and N. D. Lawrence, “Variational gaussian process dynamical systems,” in *Advances in Neural Information Processing Systems*, 2011, pp. 2510–2518.

[38] A. Damianou, M. K. Titsias, and N. Lawrence. Vargplvm software for matlab and r. [Online]. Available: https://github.com/SheffieldML/vargplvm

[39] N. Pratt, “Anatomy and kinesiology of the hand,” *Rehabilitation of the Hand and Upper Extremity*, pp. 3–17, 2011.

[40] ——, “Anatomy and kinesiology of the hand,” in *Rehabilitation of the Hand and Upper Extremity, 2-Volume Set: Expert Consult*, T. Skirven, A. Osterman, J. Fedorczyk, and P. Amadio, Eds., vol. 1. Elsevier Mosby Philadelphia PA;, 2011.

[41] I. Carpinella, P. Mazzoleni, M. Rabuffetti, R. Thorsen, and M. Ferrarin, “Experimental protocol for the kinematic analysis of the hand: definition and repeatability,” *Gait & Posture*, vol. 23, no. 4, pp. 445–454, 2006.

[42] S. K. D. J. N. T. Shibata, “Dataset of surface electromyographic (semg) signals and finger kinematics,” 2020. [Online]. Available: http://dx.doi.org/10.21227/zbkg-gy95

[43] T. S. Buchanan, D. G. Lloyd, K. Manal, and T. F. Besier, “Neuromusculoskeletal modeling: estimation of muscle forces and joint moments and movements from measurements of neural command,” *Journal of applied biomechanics*, vol. 20, no. 4, p. 367, 2004.

[44] K. Manal, R. V. Gonzalez, D. G. Lloyd, and T. S. Buchanan, “A real-time EMG-driven virtual arm,” *Computers in biology and medicine*, vol. 32, no. 1, pp. 25–36, 2002.

[45] T. Tamei and T. Shibata, "Fast reinforcement learning for three-dimensional kinetic human–robot cooperation with an EMG-to-activation model," *Advanced Robotics*, vol. 25, no. 5, pp. 563–580, 2011.

[46] J. G. Ngeo, T. Tamei, and T. Shibata, "Continuous and simultaneous estimation of finger kinematics using inputs from an EMG-to-muscle activation model," *J Neuroeng Rehabil*, vol. 11, no. 122, pp. 3–11, 2014.

[47] N. Jiang, J. L. Vest-Nielsen, S. Muceli, and D. Farina, "Emg-based simultaneous and proportional estimation of wrist/hand kinematics in uni-lateral trans-radial amputees," *Journal of neuroengineering and rehabilitation*, vol. 9, no. 1, p. 42, 2012.

[48] P. Trautman, "Manifold relevance determination: Learning the latent space of robotics," *arXiv preprint arXiv:1705.03158*, 2017.

[49] D. Shin, J. Kim, and Y. Koike, "A myokinetic arm model for estimating joint torque and stiffness from EMG signals during maintained posture," *Journal of neurophysiology*, vol. 101, no. 1, pp. 387–401, 2009.

[50] M. Atzori, A. Gijsberts, C. Castellini, B. Caputo, A.-G. M. Hager, S. Elsig, G. Giatsidis, F. Bassetto, and H. Müller, "Electromyography data for non-invasive naturally-controlled robotic hand prostheses," *Scientific data*, vol. 1, 2014.

[51] E. Bizzi and V. C. Cheung, "The neural origin of muscle synergies," *Frontiers in computational neuroscience*, vol. 7, p. 51, 2013.

[52] J. Zhao, X. Xie, X. Xu, and S. Sun, "Multi-view learning overview: Recent progress and new challenges," *Information Fusion*, vol. 38, pp. 43–54, 2017.

[53] T. Baltrusˇaitis, C. Ahuja, and L.-P. Morency, "Multimodal machine learning: A survey and taxonomy," *IEEE Transactions on Pattern Analysis and Machine Intelligence*, 2018.

[54] C. H. Ek and P. Lawrence, "Shared gaussian process latent variable models," Ph.D. dissertation, Oxford Brookes University Oxford, 2009.

[55] A. Damianou, N. D. Lawrence, and C. H. Ek, "Multi-view learning as a nonparametric nonlinear inter-battery factor analysis," *arXiv preprint arXiv:1604.04939*, 2016.

[56] J. Ngeo, T. Tamei, and T. Shibata. Dataset for surface electromyographic signals and kinematics of the hand for simultaneous and proportional finger movements. [Online]. Available: https://dynamicbrain.neuroinf.jp/modules/xoonips/detail.php?id=EMG101

[57] R. Holdefer and L. Miller, "Primary motor cortical neurons encode functional muscle synergies," *Experimental Brain Research*, vol. 146, no. 2, pp. 233–243, 2002.

[58] C. B. Hart and S. F. Giszter, "A neural basis for motor primitives in the spinal cord," *Journal of Neuroscience*, vol. 30, no. 4, pp. 1322–1336, 2010.

[59] I. Delis, E. Chiovetto, and B. Berret, "On the origins of modularity in motor control," *Journal of Neuroscience*, vol. 30, no. 22, pp. 7451–7452, 2010.

[60] T. Takei, J. Confais, S. Tomatsu, T. Oya, and K. Seki, "Neural basis for hand muscle synergies in the primate spinal cord," *Proceedings of the National Academy of Sciences*, vol. 114, no. 32, pp. 8643–8648, 2017.

[61] T. Iwasaki and T. Furukawa, "Tensor som and tensor gtm: Nonlinear tensor analysis by topographic mappings," *Neural Networks*, vol. 77, pp. 107–125, 2016.

[62] Q. Ding, J. Han, X. Zhao, and Y. Chen, "Missing-data classification with the extended full-dimensional gaussian mixture model: Applications to emg-based motion recognition," *IEEE Transactions on Industrial Electronics*, vol. 62, no. 8, pp. 4994–5005, 2015.

[63] O. Van Der Niet Otr, H. A. Reinders-Messelink, R. M. Bongers, H. Bouwsema, and C. K. Van Der Sluis, "The i-limb hand and the dmc plus hand compared: a case report," *Prosthetics and orthotics international*, vol. 34, no. 2, pp. 216–220, 2010.

[64] C. Medynski and B. Rattray, “Bebionic prosthetic design.” Myoelectric Symposium, 2011.

[65] J. T. Belter, J. L. Segil, A. M. Dollar, and R. F. Weir, “Mechanical design and performance specifications of anthropomorphic prosthetic hands: a review,” *J Rehabil Res Dev*, vol. 50, no. 5, pp. 599–618, 2013.

[66] Shadow robot. [Online]. Available: http://www.shadowrobot.com/

[67] Eh1 milano hand. [Online]. Available: http://www.prensilia.com/

[68] M. Grebenstein, “Analysis of the current state of robot hands,” in *Approaching Human Performance*. Springer, 2014, pp. 11–37.

[69] M. Ortiz-Catalan, R. Brånemark, and B. Håkansson, “Biopatrec: A modular research platform for the control of artificial limbs based on pattern recognition algorithms,” *Source code for biology and medicine*, vol. 8, no. 11, 2013.

[70] G. Naik, A. Al-Timemy, and H. Nguyen, “Transradial amputee gesture classification using an optimal number of sEMG sensors: An approach using ICA clustering,” *IEEE Trans. on Neural Syst. and Rehabil. Eng.*, 2015.

[71] M. Ison and P. Artemiadis, “Proportional myoelectric control of robots: muscle synergy development drives performance enhancement, retainment, and generalization,” *IEEE Trans. on Robotics*, vol. 31, no. 2, pp. 259–268, 2015.

[72] P. Afshar and Y. Matsuoka, “Neural-based control of a robotic hand: evidence for distinct muscle strategies,” in *IEEE Int. Conf. on Robotics and Automation*, vol. 5, 2004, pp. 4633–4638.

[73] R. Smith, F. Tenore, D. Huberdeau, R. Etienne-Cummings, and N. Thakor, “Continuous decoding of finger position from surface EMG signals for the control of powered prostheses,” in *30th Annual Int. IEEE EMBS Conference*, 2008, pp. 197–200.

[74] N. A. Shrirao, N. P. Reddy, and D. R. Kosuri, “Neural network committees for finger joint angle estimation from surface EMG signals,” *Biomedical engineering online*, vol. 8, no. 1, p. 2, 2009.

[75] M. Kaneko, K. Hayashi, P. Popovski, K. Ikeda, H. Sakai, and R. Prasad, "Amplify-and-forward cooperative diversity schemes for multi-carrier systems," *Wireless Communications, IEEE Transactions on*, vol. 7, no. 5, pp. 1845–1850, 2008.

[76] A. Krasoulis, S. Vijayakumar, and K. Nazarpour, "Evaluation of regression methods for the continuous decoding of finger movement from surface EMG and accelerometry," in *7th Int. IEEE/EMBS Conf. on Neural Eng. (NER)*. IEEE, 2015, pp. 631–634.

[77] J. Ngeo, T. Tamei, K. Ikeda, and T. Shibata, "Modeling dynamic high-dof finger postures from surface EMG using nonlinear synergies in latent space representation," in *37th IEEE EMBS Conf.*, 2015, pp. 2095–2098.

[78] M. Berniker, A. Jarc, E. Bizzi, and M. C. Tresch, "Simplified and effective motor control based on muscle synergies to exploit musculoskeletal dynamics," *Proceedings of the National Academy of Sciences*, vol. 106, no. 18, pp. 7601–7606, 2009.

[79] J. N. Ingram, K. P. Körding, I. S. Howard, and D. M. Wolpert, "The statistics of natural hand movements," *Experimental brain research*, vol. 188, no. 2, pp. 223–236, 2008.

[80] S. Deena and A. Galata, "Speech-driven facial animation using a shared gaussian process latent variable model," in *Adv. in Visual Comp.*, 2009.

[81] K. Yamane, Y. Ariki, and J. Hodgins, "Animating non-humanoid characters with human motion data," in *Proc. of the ACM SIGGRAPH/Eurographics Symposium on Computer Animation*, 2010.

[82] C. Rasmussen and H. Nickisch. Gaussian processes regression and classification toolbox version 3.1. [Online]. Available: http://gaussianprocess.org/gpml/code

[83] C. Metcalf. Southampton hand assessment procedure southampton. [Online]. Available: http://www.shap.ecs.soton.ac.uk

[84] N. Jiang, J. Vest-Nielsen, S. Muceli, and D. Farina, "EMG-based simultaneous and proportional estimation of wrist/hand kinematics in uni-lateral trans-radial amputees," *J. Neuroeng. Rehabil.*, vol. 9, 2012.

[85] J. Ngeo, T. Tamei, and T. Shibata, "Estimation of continuous multi-DOF finger joint kinematics from surface EMG using a multi-output gaussian process," in *36th Int. IEEE EMBS Conf.*, 2014.

[86] G. Gioioso, G. Salvietti, M. Malvezzi, and D. Prattichizzo, "Mapping synergies from human to robotic hands with dissimilar kinematics: an approach in the object domain," *IEEE Trans. on Robotics*, vol. 29, no. 4, pp. 825–837, 2013.

[87] J. Wang, A. Hertzmann, and D. M. Blei, "Gaussian process dynamical models," in *Adv. in NeuInfo Processing Systems*, 2005, pp. 1441–1448.

[88] N. D. Lawrence and J. Quiñonero-Candela, "Local distance preservation in the GP-LVM through back constraints," in *Proc. of the 23rd international conf. on Machine learning*. ACM, 2006, pp. 513–520.

[89] E. Todorov and Z. Ghahramani, "Analysis of the synergies underlying complex hand manipulation," in *26th Int. IEEE EMBS Conf.*, 2004.

[90] M. Ison and P. Artemiadis, "The role of muscle synergies in myoelectric control: trends and challenges for simultaneous multifunction control," *Journal of neural engineering*, vol. 11, no. 5, p. 051001, 2014.

[91] L. H. Ting and S. A. Chvatal, "Decomposing muscle activity in motor tasks," *Motor Control Theories, Experiments and Applications. Oxf. Univ. Press, New York*, pp. 102v–138, 2010.

[92] K. Nazarpour, A. Barnard, and A. Jackson, "Flexible cortical control of task-specific muscle synergies," *The Journal of Neuroscience*, vol. 32, no. 36, pp. 12 349–12 360, 2012.

[93] J. Ngeo, T. Tamei, and T. Shibata, "Continuous estimation of finger joint angles using muscle activation inputs from surface EMG signals," in *34th International IEEE EMBS Conference*, 2012, pp. 2756–2759.

[94] P. J. Kyberd, A. Murgia, M. Gasson, T. Tjerks, C. Metcalf, P. H. Chappell, K. Warwick, S. E. Lawson, and T. Barnhill, "Case studies to demonstrate the range of applications of the southampton hand assessment procedure," *The British Journal of Occupational Therapy*, vol. 72, no. 5, pp. 212–218, 2009.

[95] M. Hirashima and T. Oya, "How does the brain solve muscle redundancy? filling the gap between optimization and muscle synergy hypotheses," *Neuroscience research*, vol. 104, pp. 80–87, 2016.

[96] N. Bhatt and S. Varadhan, "Hand posture comparison in synergy space," *PeerJ PrePrints*, 2017.

[97] S. Israely, G. Leisman, C. C. Machluf, and E. Carmeli, "Muscle synergies control during hand-reaching tasks in multiple directions post-stroke," *Frontiers in Computational Neuroscience*, vol. 12, p. 10, 2018.

[98] J. H. Ham, D. D. Lee, and L. K. Saul, "Learning high dimensional correspondences from low dimensional manifolds," 2003.

[99] A. d'Avella and E. Bizzi, "Shared and specific muscle synergies in natural motor behaviors," *Proceedings of the National Academy of Sciences of the United States of America*, vol. 102, no. 8, pp. 3076–3081, 2005.

[100] I. Delis, S. Panzeri, T. Pozzo, and B. Berret, "A unifying model of concurrent spatial and temporal modularity in muscle activity," *Journal of Neurophysiology*, vol. 111, no. 3, pp. 675–693, 2013.

[101] M. Santello, M. Bianchi, M. Gabiccini, E. Ricciardi, G. Salvietti, D. Prattichizzo, M. Ernst, A. Moscatelli, H. Jörntell, A. M. Kappers *et al.*, "Hand synergies: integration of robotics and neuroscience for understanding the control of biological and artificial hands," *Physics of life reviews*, vol. 17, pp. 1–23, 2016.

[102] D. H. Hubel, "Receptive field of single neurons in the cat's striate cortex," *J Physiol (Lond)*, vol. 148, pp. 574–591, 1959.

[103] F. Lacquaniti, Y. P. Ivanenko, and M. Zago, "Development of human locomotion," *Current opinion in neurobiology*, vol. 22, no. 5, pp. 822–828, 2012.

[104] N. Dominici, Y. P. Ivanenko, G. Cappellini, A. d'Avella, V. Mond`ı, M. Cicchese, A. Fabiano, T. Silei, A. Di Paolo, C. Giannini *et al.*, "Locomotor primitives in newborn babies and their development," *Science*, vol. 334, no. 6058, pp. 997–999, 2011.

[105] J. J. Kutch, A. D. Kuo, A. M. Bloch, and W. Z. Rymer, "Endpoint force fluctuations reveal flexible rather than synergistic patterns of muscle cooperation," *Journal of neurophysiology*, vol. 100, no. 5, pp. 2455–2471, 2008.

[106] F. J. Valero-Cuevas, M. Venkadesan, and E. Todorov, "Structured variability of muscle activations supports the minimal intervention principle of motor control," *Journal of neurophysiology*, vol. 102, no. 1, pp. 59–68, 2009.

[107] N. Bernstein, "The co-ordination and regulation of movements," *The co-ordination and regulation of movements*, 1966.

[108] H. Broer and F. Takens, *Dynamical systems and chaos*. Springer Science & Business Media, 2010, vol. 172.

[109] G. Rasool, K. Iqbal, N. Bouaynaya, and G. White, "Real-time task discrimination for myoelectric control employing task-specific muscle synergies," *IEEE Transactions on Neural Systems and Rehabilitation Engineering*, vol. 24, no. 1, pp. 98–108, 2016.

[110] G. Torres-Oviedo and L. H. Ting, "Subject-specific muscle synergies in human balance control are consistent across different biomechanical contexts," *Journal of neurophysiology*, vol. 103, no. 6, pp. 3084–3098, 2010.

[111] I. Nabney and C. Bishop. Netlab neural network software. [Online]. Available: http://www1.aston.ac.uk/eas/research/groups/ncrg/resources

[112] K. Xu, H. Liu, Y. Du, and X. Zhu, "A comparative study for postural synergy synthesis using linear and nonlinear methods," *International Journal of Humanoid Robotics*, vol. 13, no. 03, p. 1650009, 2016.

[113] A. d'Avella, A. Portone, and F. Lacquaniti, "Superposition and modulation of muscle synergies for reaching in response to a change in target location," *Journal of neurophysiology*, vol. 106, no. 6, pp. 2796–2812, 2011.

[114] J. Taborri, V. Agostini, P. K. Artemiadis, M. Ghislieri, D. A. Jacobs, J. Roh, and S. Rossi, “Feasibility of muscle synergy outcomes in clinics, robotics, and sports: A systematic review,” *Applied bionics and biomechanics*, vol. 2018, 2018.

[115] A. Krasoulis, “Machine learning-based dexterous control of hand prostheses,” 2018.

Publication List

Peer-reviewed Journal Paper

1. Dwivedi, Sanjay Kumar , Ngeo, Jimson, and Shibata, Tomohiro. Extraction of nonlinear synergies for proportional and simultaneous estimation of finger kinematics. IEEE Transactions of Biomedical Engineering (TBME), 2020.

International Conferences

1. Dwivedi, Sanjay Kumar and Shibata, Tomohiro. An Approach to Extract Nonlinear Muscle Synergies from sEMG through Multi-Model Learning. 41th IEEE-EMBC, 2019.

Domestic Conferences

1. Dwivedi, Sanjay Kumar , Koganthi Nishanth, and Shibata Tomohiro. Missing value estimation of sEMG signals using BGPLVM toward control of a multi-fingered prosthetic hand. Japanese Neural Network Society (JNNS), 2016.